NASA
Technical
Paper
2649

March 1987

Exploiting Symmetries in the Modeling and Analysis of Tires

Ahmed K. Noor,
Carl M. Andersen,
and John A. Tanner

NASA

NASA Technical Paper 2649

1987

Exploiting Symmetries in the Modeling and Analysis of Tires

Ahmed K. Noor
The George Washington University
Joint Institute for Advancement of Flight Sciences
Langley Research Center
Hampton, Virginia

Carl M. Andersen
The College of William and Mary
Williamsburg, Virginia

John A. Tanner
Langley Research Center
Hampton, Virginia

National Aeronautics and Space Administration

Scientific and Technical Information Branch

CONTENTS

SUMMARY

Three basic types of symmetry (and their combinations) exhibited by tire response are identified. A simple and efficient computational strategy is presented for reducing both the size of the model and the cost of the analysis of tires in the presence of symmetry-breaking conditions (e.g., unsymmetry of the tire material, geometry, and/or loading). The strategy is based on *approximation* of the unsymmetric response of the tire with a *linear combination of symmetric and antisymmetric global approximation vectors (or modes)*.

The three main elements of the computational strategy are as follows: (1) use of three-field mixed finite-element models having independent shape functions for stress resultants, strain components, and generalized displacements, with the stress resultants and the strain components allowed to be discontinuous at interelement boundaries; (2) use of operator splitting (additive decomposition of some of the matrices and vectors in the finite-element model) to delineate the symmetric and antisymmetric contributions to the response; and (3) successive use of the finite-element method and the classic Rayleigh-Ritz technique to substantially reduce the number of degrees of freedom. The finite-element method is first used to generate a few global approximation vectors (or modes). Then the amplitudes of these modes are computed with the Rayleigh-Ritz technique.

The proposed computational strategy is applied to three quasi-symmetric problems of tires, namely, (1) linear analysis of anisotropic tires through use of semianalytic finite elements, (2) nonlinear analysis of anisotropic tires through use of two-dimensional shell finite elements, and (3) nonlinear analysis of orthotropic tires subjected to unsymmetric loading. In the first two applications, the anisotropy (nonorthotropy) of the tire is the source of the symmetry breaking; in the third application, the quasi-symmetry is due to the unsymmetry of the loading. The effectiveness of the proposed computational strategy is also demonstrated with numerical examples, and its potential for handling practical tire problems is outlined.

1 INTRODUCTION

One of the most challenging applications of computational structural mechanics is the numerical simulation of the response of aircraft tires during taxi, take-off, and landing operations. In addition to the harsh environment tires are subjected to, their composite structure is composed of rubber and textile constituents which exhibit anisotropic, nonhomogeneous material properties. (See fig. 1.) Tires are subjected to inflation pressure and to a variety of unsymmetric mechanical and thermal loads which can result in large structural rotations and deformations as well as in variations in the characteristics of the tire constituents. Also, the laminated carcass of aircraft tires is thick enough to allow significant transverse-shear deformations. Moreover, the detailed stress and temperature distributions in tires may require the use of three-dimensional finite elements to model certain regions of the tire. To date only a few analytical tools have been available to assist the tire designer. A review of the commonly used models for predicting tire response is given in references 1 to 3.

The aforementioned difficulties can make the cost of the numerical simulation of the tire response prohibitive. Hence, there is a need to develop modeling strategies and analysis methods to reduce this expense. In recent years nonlinear analyses of static and dynamic problems have become the focus of extensive research

efforts. This endeavor has prompted the development of versatile and powerful finite-element discretization methods as well as the development of improved numerical methods and software systems for nonlinear static and dynamic analyses of structures and solids. Novel techniques which have emerged from these efforts include three-field mixed finite-element models (refs. 4 and 5), semianalytic finite-element models for shells of revolution (refs. 6 and 7), techniques for exploiting the special symmetries exhibited by anisotropic plates and shells in their finite-element analyses (refs. 8 and 9), single- and multiple-parameter reduction techniques (refs. 10 to 13), and operator splitting techniques (refs. 14 to 16). Current tire modeling studies at NASA Langley Research Center are aimed at developing an accurate and cost-effective computational strategy for predicting tire response. This is accomplished through combining the aforementioned analysis techniques with a modeling strategy for exploiting the symmetries exhibited by the tire response. In situations for which the symmetry is broken because of unsymmetry of the tire material, geometry, or loading (quasi-symmetric problems), the proposed strategy allows the reduction of the size of the analysis model to that of the corresponding symmetric tire problem.

The objectives of the present paper are the following: (1) to review the different types of symmetry exhibited by the tire response; (2) to present a simple and efficient computational strategy for the analysis of tires in the presence of symmetry-breaking conditions; and (3) to discuss the potential of the proposed computational strategy and its application to practical tire problems. To sharpen the focus of the study, discussion is limited to tires with elliptic cross sections and linear material response. The tire is modeled through use of the moderate-rotation, geometrically nonlinear Sanders-Budiansky shell theory with the effects of transverse-shear deformation and laminated anisotropic material response included (refs. 17 and 18). The sign convention for the external loading, generalized displacements, and stress resultants is given in figure 2.

2 SYMMETRIES EXHIBITED BY TIRE RESPONSE

The fundamental definitions of symmetry, symmetry elements, and symmetry operations are reviewed in reference 19. When applied to tires, the "axiom of symmetry" introduced in references 19 and 20 becomes the following: given a tire exhibiting certain types of symmetry and a system of loads which exhibits the same types of symmetry as those of the tire, the response obtained is expected to exhibit the same types of symmetry as those inherent in the tire and the loading system. Herein the symmetry of the tire refers to the symmetry of (1) tire geometry, (2) lamination and material parameters (e.g., cord orientation and stacking of layers), and (3) boundary conditions at the rim.

The symmetry of tires is described by giving the set of all operations which preserve the distance between pairs of points of the tire and which take the tire into an equivalent configuration (i.e., into a configuration which is indistinguishable from the original configuration but not necessarily identical to that configuration). Any such operation is called a symmetry transformation. The set of all symmetry transformations forms the symmetry group of the tire (ref. 20).

The three basic types of symmetry frequently exhibited by the tire response are (1) axial symmetry, (2) rotational symmetry, and (3) reflection symmetry. The characteristics of these symmetries are examined subsequently.

2.1 Axial Symmetry

A tire is said to exhibit axial symmetry about its axis of revolution (y-axis in fig. 3) if it can be brought into an equivalent configuration by any rotation about that axis. Axial symmetry is exhibited by tires whose geometry, material properties, and boundary conditions are independent of the circumferential coordinate θ (i.e., the tire is axisymmetric). If the loading is also axisymmetric, then the response is expected to be axisymmetric. (This excludes the case of unsymmetric buckling of a tire subjected to axisymmetric loading.) For isotropic and orthotropic tires subjected to axisymmetric loading, the two sets of generalized displacements, strain components, and stress resultants (u, w, ϕ_s; ε_s, ε_θ, κ_θ, $2\varepsilon_{s3}$; and N_s, N_θ, M_s, M_θ, Q_s and v, ϕ_θ; $2\varepsilon_{s\theta}$, $2\kappa_{s\theta}$, $2\varepsilon_{\theta 3}$; and $N_{s\theta}$, $M_{s\theta}$, Q_θ) are generally uncoupled. In contradistinction, for anisotropic tires (also subjected to axisymmetric loading) the two sets are coupled. (See fig. 4.) In the presence of axial symmetry only one meridian of the tire needs to be analyzed. (See fig. 4.)

2.2 Rotational Symmetry

A tire exhibits rotational symmetry about an axis normal to the axis of revolution (e.g., x-axis or z-axis in fig. 3) if a 180° rotation around this axis brings the tire into an equivalent configuration. Such rotations are referred to as dihedral rotations, in contradistinction to the axial rotation discussed in section 2.1. If the external loading exhibits rotational symmetry about the same axis as the tire, then the response will also exhibit the same symmetry. For convenience, the reference (middle) surface of the tire is parametrized by the two coordinates ξ and θ. (See fig. 3.) The coordinate ξ represents a normalized arc length distance measured from the crown of the tire, and the coordinate θ is the circumferential angle measured from the intersection of the negative z-axis with the reference surface. The rotational symmetry of the external loading and the response about an axis normal to the tire through the origin ($\xi = \theta = 0$, the z-axis in fig. 3) are expressed by the following relations:

External loading:

$$\begin{Bmatrix} p_s \\ p_\theta \\ p \\ m_s \\ m_\theta \end{Bmatrix}_{(\xi,\theta)} = \begin{Bmatrix} -p_s \\ -p_\theta \\ p \\ -m_s \\ -m_\theta \end{Bmatrix}_{(-\xi,-\theta)} \tag{1}$$

Generalized displacements:

$$\begin{Bmatrix} u \\ v \\ w \\ \phi_s \\ \phi_\theta \end{Bmatrix}_{(\xi,\theta)} = \begin{Bmatrix} -u \\ -v \\ w \\ -\phi_s \\ -\phi_\theta \end{Bmatrix}_{(-\xi,-\theta)} \tag{2}$$

Stress resultants:

$$\begin{Bmatrix} N_s \\ N_\theta \\ N_{s\theta} \\ M_s \\ M_\theta \\ M_{s\theta} \\ Q_s \\ Q_\theta \end{Bmatrix}_{(\xi,\theta)} = \begin{Bmatrix} N_s \\ N_\theta \\ N_{s\theta} \\ M_s \\ M_\theta \\ M_{s\theta} \\ -Q_s \\ -Q_\theta \end{Bmatrix}_{(-\xi,-\theta)} \tag{3}$$

where p_s, p_θ, and p represent the intensities of the loading in the s-, θ-, and x_3-directions to the reference surface and m_s and m_θ are the intensities of the applied moments.

The symmetry relations for the strain components are the same as those for the corresponding stress resultants. These relations show that for a symmetric loading (defined by eqs. (1)), the generalized displacements u, v, ϕ_s, and ϕ_θ, the transverse-shear stress resultants Q_s and Q_θ, and the transverse-shear strain components $2\varepsilon_{s3}$ and $2\varepsilon_{\theta 3}$ vanish at the axis of rotation ($\xi = \theta = 0$).

Rotational symmetry can be exhibited by isotropic, orthotropic, and anisotropic tires. It is sometimes referred to in the literature as *inversion symmetry* because of its effect on the (ξ,θ) space. The intersections of the axis of rotational symmetry with the tire middle surface correspond to the *centers of symmetry* in the (ξ,θ) space.

An illustration of rotational symmetry for a two-layered tire subjected to uniform inflation pressure and a localized loading is given in figure 5(a), in which normalized contour plots for the two displacements v and w are shown. As can be seen from figure 5(a), only one-half of the tire needs to be analyzed.

2.3 Reflection Symmetry

A tire exhibits reflection (or mirror) symmetry with respect to a plane (e.g.,

x-z plane in fig. 3) if it can be brought into an equivalent configuration by mirror reflection in that plane. For reflection symmetry with respect to the plane $\xi = 0$ (fig. 3), the symmetry relations for the tire loading and response are given by the following:

External loading:

$$\begin{Bmatrix} p_s \\ p_\theta \\ p \\ m_s \\ m_\theta \end{Bmatrix}_{(\xi,\theta)} = \begin{Bmatrix} -p_s \\ p_\theta \\ p \\ -m_s \\ m_\theta \end{Bmatrix}_{(-\xi,\theta)} \tag{4}$$

Generalized displacements:

$$\begin{Bmatrix} u \\ v \\ w \\ \phi_s \\ \phi_\theta \end{Bmatrix}_{(\xi,\theta)} = \begin{Bmatrix} -u \\ v \\ w \\ -\phi_s \\ \phi_\theta \end{Bmatrix}_{(-\xi,\theta)} \tag{5}$$

Stress resultants:

$$\begin{Bmatrix} N_s \\ N_\theta \\ N_{s\theta} \\ M_s \\ M_\theta \\ M_{s\theta} \\ Q_s \\ Q_\theta \end{Bmatrix}_{(\xi,\theta)} = \begin{Bmatrix} N_s \\ N_\theta \\ -N_{s\theta} \\ M_s \\ M_\theta \\ -M_{s\theta} \\ -Q_s \\ Q_\theta \end{Bmatrix}_{(-\xi,\theta)} \tag{6}$$

The symmetry relations for the strain components are the same as those for the corresponding stress resultants. Reflection symmetry can occur in isotropic and orthotropic tires but not in anisotropic tires.

2.4 Symmetry Combinations

Combinations of the foregoing three basic types of symmetry are possible in tire response. These combinations reduce the size of the analysis model and the associated computational cost beyond what is possible with only one symmetry

transformation. The symmetry combinations can be of the same type or of different types. The following three examples of symmetry combinations are discussed herein.

2.4.1 Reflection symmetry combined with dihedral rotational symmetry.- This results in reflection symmetry with respect to two planes, as shown in figure 5(b) for a two-layered orthotropic tire subjected to uniform inflation pressure and localized loading. The size of the analysis model is only one quadrant of the tire.

2.4.2 Periodic (or translational) symmetry.- Periodic symmetry is rotational symmetry around both the x- and the z-axis (see fig. 3) and is exhibited by the response of orthotropic and anisotropic tires, for which the tire geometry, material, boundary conditions, and loading have rotational symmetry around both axes. An example of periodic symmetry for two-layered orthotropic tires subjected to uniform inflation pressure and "symmetric" localized loading is given in figure 5(c). The size of the analysis model is only one octant of the tire.

2.4.3 Axial symmetry combined with rotational and/or reflection symmetry.- If both the tire and the loading possess rotational and/or reflection symmetry in addition to axial symmetry, then the size of the analysis model reduces to half the meridian. The symmetry conditions in these cases are listed in table 1.

2.5 Linear Response of Tires Subjected to Unsymmetric Loading

The aforementioned symmetry concepts can be used in predicting the linear response of tires subjected to unsymmetric loading. This is accomplished through the decomposition of the loading into various symmetric and antisymmetric components. The tire response is then obtained through summation of the responses to each of the symmetric and antisymmetric loading components. These responses have *a priori* known symmetries (and/or antisymmetries), and therefore only a small portion of the tire needs to be analyzed in each case, with a consequent large reduction in the computational effort.

Note that *a unique correspondence exists between the symmetric and antisymmetric components of the loading and the corresponding response components*. This is based on the principle of superposition, which is generally valid only for linear problems.

3 SYMMETRY-BREAKING (QUASI-SYMMETRY) CONDITIONS

Symmetry-breaking, or quasi-symmetry, conditions are used in the present study for situations in which the tire response *cannot be exactly computed as a finite sum of symmetric and antisymmetric modes*. The major sources of symmetry breaking are unsymmetry of the tire material, geometry, boundary conditions, and loading. In the mechanics literature the term "asymmetry" is often used to denote unsymmetry. Material anisotropy is a source of reflection unsymmetry. The unsymmetry in geometry can be caused by the presence of unsymmetric imperfections in the tire. The contact of the tire with the pavement can be considered as unsymmetric boundary conditions. Unsymmetric loading is a source of symmetry breaking when the nonlinear tire response is considered. In a practical situation, a combination of the different types of unsymmetry may exist.

If the unsymmetry of the tire material, geometry, or loading is small, the unsymmetric tire response can be obtained as a small perturbation from the corresponding symmetric response. As an example of this, for "slightly anisotropic" tires

the response can be obtained as a small perturbation from the orthotropic response (see refs. 21 and 22), thereby reducing the size of the analysis model of the anisotropic tire to that of the corresponding orthotropic tire. On the other hand, when the unsymmetry is large (e.g., for strongly anisotropic tires), the classic perturbation technique does not work. In section 4, a computational strategy is presented for reducing the size of the analysis model for quasi-symmetric problems of tires to that of the corresponding symmetric problems.

4 PROPOSED COMPUTATIONAL STRATEGY FOR QUASI-SYMMETRIC PROBLEMS

In this section a computational strategy is presented for the efficient analysis of tires in the presence of symmetry-breaking (quasi-symmetric) conditions. The proposed strategy is based on *approximating the unsymmetric response* of the tire with a *linear combination of symmetric and antisymmetric global approximation vectors* (or modes). The three main elements of the computational strategy are as follows: (1) use of three-field mixed models having independent shape functions for stress resultants, strain components, and generalized displacements, with the stress resultants and strain components allowed to be discontinuous at interelement boundaries; (2) use of operator splitting (additive decomposition of some of the matrices and vectors used in the finite-element model) to delineate the symmetric and antisymmetric contributions to the response; and (3) successive use of the finite-element method and the classic Rayleigh-Ritz technique to substantially reduce the number of degrees of freedom. The finite-element method is first used to generate *a few* global approximation vectors (or modes). Then the amplitudes of these modes are computed with the Rayleigh-Ritz technique.

Main elements 2 and 3 are essential for the success of the computational strategy, and main element 1 significantly enhances the efficiency and effectiveness of the strategy. In sections 5 to 7 the details of application of the proposed strategy to the following three quasi-symmetric problems are discussed: linear analysis of anisotropic tires (subjected to arbitrary loading) through use of semianalytic finite elements; nonlinear analysis of anisotropic tires through use of two-dimensional shell finite elements; and nonlinear analysis of orthotropic tires subjected to unsymmetric loading. In the first two applications the anisotropy (nonorthotropy) of the tire is the source of symmetry breaking; in the third application, the symmetry breaking is due to the unsymmetry of the loading. Numerical results are presented in section 8.

The three applications presented in sections 5 to 7 are intended to demonstrate the use of the proposed computational strategy in analyzing practical tire problems. Tires with a small number of plies (e.g., two) generally exhibit a high degree of anisotropy. As the number of plies in the tire increases, the effect of the anisotropic (nonorthotropic) stiffness coefficients on the tire response decreases, and for 10 or more plies the tire can be treated as orthotropic.

For tires with uniform circumferential properties subjected to pressure loading, the response can be accurately predicted with the linear theory. If the loading is nonuniform in the circumferential direction, then an efficient analysis technique can be obtained from a Fourier series representation of the different tire quantities in the circumferential direction and a one-dimensional finite-element discretization in the meridional direction. However, for anisotropic tires this analysis technique can become expensive. The application of the aforementioned computational strategy significantly reduces the cost of analyzing highly anisotropic tires, as described in section 5.

When the tires are subjected to a combination of pressure loading and localized loading (e.g., in the contact region), then the use of two-dimensional shell finite elements is appropriate. However, this technique can also become quite expensive for anisotropic tires or for unsymmetric localized loading. The use of the computational strategy to reduce the cost of the analysis in these cases is discussed in sections 6 and 7.

The computational strategy is based on a form of the moderate-rotation Sanders-Budiansky shell theory with the effects of transverse-shear deformation and laminated, anisotropic material response included. (See refs. 17 and 18 and appendix A.) A total Lagrangian formulation is used and the fundamental unknowns consist of the five generalized displacements, the eight stress resultants, and the corresponding eight strain components of the middle surface. (See fig. 2 for sign convention.)

5 LINEAR ANALYSIS OF ANISOTROPIC TIRES THROUGH USE OF SEMIANALYTIC FINITE ELEMENTS

For tires with uniform circumferential properties, an approach generally used for predicting the linear response is based on the representation of the shell variables and the external loadings with Fourier series in the circumferential coordinate θ combined with the use of finite elements in the meridional direction. (See ref. 23.) The following expressions are used for the external loadings:

$$\begin{Bmatrix} p_s(s,\theta) \\ p_\theta(s,\theta) \\ p(s,\theta) \\ m_s(s,\theta) \\ m_\theta(s,\theta) \end{Bmatrix} = \sum_{n=0}^{\infty} N^i \begin{Bmatrix} p^i_{s,n} \\ -p^i_{\theta,n} \\ p^i_n \\ m^i_{s,n} \\ -m^i_{\theta,n} \end{Bmatrix} \cos n\theta + \sum_{n=1}^{\infty} N^i \begin{Bmatrix} \bar{p}^i_{s,n} \\ \bar{p}^i_{\theta,n} \\ \bar{p}^i_n \\ \bar{m}^i_{s,n} \\ \bar{m}^i_{\theta,n} \end{Bmatrix} \sin n\theta \tag{7}$$

The generalized displacements X, stress resultants H, and strain components E are approximated with expressions of the form

$$X(s,\theta) = \sum_{n=0}^{\infty} N^i X^i_n \cos n\theta + \sum_{n=1}^{\infty} N^i \bar{X}^i_n \sin n\theta \tag{8}$$

$$H(s,\theta) = \sum_{n=0}^{\infty} \bar{N}^i H^i_n \cos n\theta + \sum_{n=1}^{\infty} \bar{N}^i \bar{H}^i_n \sin n\theta \tag{9}$$

$$E(s,\theta) = \sum_{n=0}^{\infty} \bar{N}^i E^i_n \cos n\theta + \sum_{n=1}^{\infty} \bar{N}^i \bar{E}^i_n \sin n\theta \tag{10}$$

where N^i are the shape functions used in approximating the generalized displacements in the meridional direction; $\bar{N}^i$ are the shape functions used in approximating the stress resultants and the strain components; X^i_n and $\bar{X}^i_n$ refer to the generalized nodal displacement coefficients associated with the Fourier harmonic n; H^i_n

and $\bar{H}_n^{\bar{i}}$ refer to the stress-resultant parameters associated with the harmonic n; and E_n^i and $\bar{E}_n^{\bar{i}}$ refer to the strain parameters associated with the harmonic n. The barred tire quantities are associated with the sine series. Based on the present study, the degree of polynomial shape functions $\bar{N}^{\bar{i}}$ is one lower than that of N^i. Moreover, the continuity of the stress resultants and the strain components is not imposed at the interelement boundaries and, therefore, both the strain parameters and the stress-resultant parameters can be eliminated at the element level.

In equations (7) to (10), the range of the superscript i is 1 to m, the number of displacement nodes in the element; the range of superscript $\bar{i}$ is 1 to δ, the number of parameters used in approximating each of the stress resultants or the strain components. A repeated superscript denotes summation over its entire range.

5.1 Governing Finite-Element Equations

The governing finite-element equations are obtained through application of the three-field Hu-Washizu mixed variational principle. For tires with uniform circumferential properties, the finite-element equations uncouple in harmonics, that is, each load harmonic excites only the response in the same harmonic. For the harmonic n, the governing equations for individual elements can be cast in the following form:

$$\begin{bmatrix} K & R & 0 \\ R^t & 0 & S \\ 0 & S^t & 0 \end{bmatrix}_n \begin{Bmatrix} E \\ H \\ X \end{Bmatrix}_n - \begin{Bmatrix} 0 \\ 0 \\ Q \end{Bmatrix}_n = 0 \tag{11}$$

where $\{X\}_n$, $\{E\}_n$, and $\{H\}_n$ are respectively the vectors of nodal displacement coefficients, the strain parameters, and the stress-resultant parameters associated with n; $[K]_n$, $[R]_n$, and $[S]_n$ are "generalized" stiffness matrices; $\{Q\}_n$ is the vector of normal external loadings; subscript n refers to the nth Fourier harmonic; and superscript t denotes transposition.

If the strain parameters are eliminated from equations (11) on the element level, one obtains the governing equations of the two-field Hellinger-Reissner mixed models. The governing equations for the individual elements of these models take the form

$$\begin{bmatrix} -F & S \\ S^t & 0 \end{bmatrix}_n \begin{Bmatrix} H \\ X \end{Bmatrix}_n = \begin{Bmatrix} 0 \\ Q \end{Bmatrix}_n = 0 \tag{12}$$

where $[F]$ is the linear flexibility matrix of the element given by

$$[F] = [R]^t[K]^{-1}[R]$$

The equivalence between the three-field Hu-Washizu mixed models, the two-field Hellinger-Reissner mixed models, and the reduced-selective integration displacement models is discussed in references 4 and 24.

5.2 Operator Splitting

To simplify the analysis of anisotropic tires, the vectors $\{E\}_n$, $\{H\}_n$, $\{X\}_n$, and $\{Q\}_n$ in equations (11) are each partitioned into two subvectors: $\{\mathfrak{E}\}_n$, $\{E\}_n$; $\{\mathfrak{H}\}_n$, $\{H\}_n$; $\{\mathfrak{X}\}_n$, $\{X\}_n$; and $\{\mathfrak{Q}\}_n$, $\{Q\}_n$. The first and second subvectors of each pair are associated with the symmetric and antisymmetric fundamental unknowns (or external loadings), respectively. The two sets of symmetric and antisymmetric shell variables are listed in table 2. In table 2, the shell variables without a bar are the coefficients of the cosine series, and the barred tire variables are the coefficients of the sine series. (See eqs. (8), (9), and (10).)

The matrix $[K]_n$ in equations (11) is now partitioned into two block-diagonal submatrices $[\mathfrak{K}]_n$ and $[K]_n$, associated with $\{\mathfrak{E}\}_n$ and $\{E\}_n$, respectively, and a coupling submatrix $[\bar{K}]_n$. The coupling submatrix contains all the nonorthotropic material stiffnesses of the tire and, therefore, vanishes for orthotropic (and isotropic) tires.

The matrices $[R]_n$ and $[S]_n$ are similarly partitioned into the submatrices $[\mathfrak{R}]_n$, $[R]_n$ and $[\mathfrak{S}]_n$, $[S]_n$ associated with $\{\mathfrak{E}\}_n$, $\{\mathfrak{H}\}_n$, $\{\mathfrak{X}\}_n$ and $\{E\}_n$, $\{H\}_n$, $\{X\}_n$. No coupling submatrices other than $[\bar{K}]_n$ exist between the two sets.

The governing finite-element equations for each individual element are partitioned into two sets of coupled equations and are embedded into a single-parameter family of equations of the form

$$\begin{bmatrix} \mathfrak{K} & \mathfrak{R} & 0 \\ \mathfrak{R}^t & 0 & \mathfrak{S} \\ 0 & \mathfrak{S}^t & 0 \end{bmatrix}_n \begin{Bmatrix} \mathfrak{E} \\ \mathfrak{H} \\ \mathfrak{X} \end{Bmatrix}_n + \lambda \begin{bmatrix} \bar{K} & 0 & 0 \\ 0 & 0 & 0 \\ 0 & 0 & 0 \end{bmatrix}_n \begin{Bmatrix} E \\ H \\ X \end{Bmatrix}_n - \begin{Bmatrix} 0 \\ 0 \\ \mathfrak{Q} \end{Bmatrix}_n = 0 \tag{13}$$

and

$$\begin{bmatrix} K & R & 0 \\ R^t & 0 & S \\ 0 & S^t & 0 \end{bmatrix}_n \begin{Bmatrix} \mathfrak{E} \\ H \\ X \end{Bmatrix}_n + \lambda \begin{bmatrix} \bar{K}^t & 0 & 0 \\ 0 & 0 & 0 \\ 0 & 0 & 0 \end{bmatrix}_n \begin{Bmatrix} \mathfrak{E} \\ \mathfrak{H} \\ \mathfrak{X} \end{Bmatrix}_n - \begin{Bmatrix} 0 \\ 0 \\ Q \end{Bmatrix}_n = 0 \tag{14}$$

In equations (13) and (14), λ is a tracing parameter which identifies all the nonorthotropic (anisotropic) contributions contained in the matrix $[K]_n$. For $\lambda = 0$, equations (13) and (14) are uncoupled; that is, the response to symmetric loading is uncoupled from the response to antisymmetric loading.

The explicit forms of the arrays appearing in equations (13) and (14) are given in appendix B. For $n > 0$, $[\mathfrak{K}]_n = [K]_n$, $[\mathfrak{R}]_n = [R]_n$, $[\mathfrak{S}]_n = [S]_n$, and $[\bar{K}]_n = [\bar{K}]_n^t$.

5.3 Application of Reduction Method

A reduction method is now applied to uncouple governing equations (13) and (14) and to reduce the total number of degrees of freedom of the initial discretization.

The method is based on generating a few global approximation vectors or modes at $\lambda = 0$ with the finite model. The vectors of nodal displacement coefficients, stress-resultant parameters, and strain parameters are then expressed as linear combinations of these global approximation vectors in the following transformation:

$$\begin{Bmatrix} \mathfrak{E} \\ \mathfrak{H} \\ \mathfrak{X} \end{Bmatrix}_n = \begin{bmatrix} \Gamma_{\mathfrak{E}} \\ \Gamma_{\mathfrak{H}} \\ \Gamma_{\mathfrak{X}} \end{bmatrix}_n \{\psi\}_n \tag{15}$$

and

$$\begin{Bmatrix} E \\ H \\ X \end{Bmatrix}_n = \begin{bmatrix} \Gamma_E \\ \Gamma_H \\ \Gamma_X \end{bmatrix}_n \{\psi\}_n \tag{16}$$

where the matrices $[\Gamma]_n$ are transformation matrices and $\{\psi\}_n$ is a vector of undetermined coefficients (amplitudes of global approximation vectors) which are functions of λ.

An effective choice for the global approximation vectors (the columns of the matrices $[\Gamma]_n$) consists of the solution corresponding to $\lambda = 0$ and its various-order derivatives with respect to λ (evaluated at $\lambda = 0$), that is,

$$[\Gamma_{\mathfrak{E}}]_n = \left[\{\mathfrak{E}\}_n \quad \{\frac{\partial \mathfrak{E}}{\partial \lambda}\}_n \quad \left\{\frac{\partial^2 \mathfrak{E}}{\partial \lambda^2}\right\}_n \quad \cdots \quad \left\{\frac{\partial^{r-1} \mathfrak{E}}{\partial \lambda^{r-1}}\right\}_n \right] \tag{17}$$

$$[\Gamma_{\mathfrak{H}}]_n = \left[\{\mathfrak{H}\}_n \quad \{\frac{\partial \mathfrak{H}}{\partial \lambda}\}_n \quad \left\{\frac{\partial^2 \mathfrak{H}}{\partial \lambda^2}\right\}_n \quad \cdots \quad \left\{\frac{\partial^{r-1} \mathfrak{H}}{\partial \lambda^{r-1}}\right\}_n \right] \tag{18}$$

$$[\Gamma_{\mathfrak{X}}]_n = \left[\{\mathfrak{X}\}_n \quad \{\frac{\partial \mathfrak{X}}{\partial \lambda}\}_n \quad \left\{\frac{\partial^2 \mathfrak{X}}{\partial \lambda^2}\right\}_n \quad \cdots \quad \left\{\frac{\partial^{r-1} \mathfrak{X}}{\partial \lambda^{r-1}}\right\}_n \right] \tag{19}$$

with similar expressions for $[\Gamma_E]_n$, $[\Gamma_H]_n$, and $[\Gamma_X]_n$ in terms of $\{E\}$, $\{H\}$, and $\{X\}$. The total number of global approximation vectors is r.

The equations used in generating the global approximation vectors are obtained by successive differentiation of the finite-element equations of the discretized shell (eqs. (13) and (14)) and are listed in appendix C. The global approximation vectors are generated at $\lambda = 0$, thereby uncoupling equations (13) and (14).

For symmetric loadings the vectors $\{E\}$, $\{H\}$, $\{X\}$, and all their even-order derivatives with respect to λ are zero. Also, the odd-order derivatives of $\{\mathfrak{E}\}$, $\{\mathfrak{H}\}$, and $\{\mathfrak{X}\}$ with respect to λ vanish. For antisymmetric loadings, the situation is reversed with respect to the derivatives of $\{E\}$, $\{H\}$, and $\{X\}$ and of $\{\mathfrak{E}\}$, $\{\mathfrak{H}\}$, and $\{\mathfrak{X}\}$.

The classic Rayleigh-Ritz technique is used to replace the governing finite-element equations of the shell with the following reduced system of equations in the unknown parameters (components of the vector $\{\psi\}_n$):

$$\left[[\tilde{k}]_n + \lambda[\tilde{k}]_n\right]\{\psi\}_n = \{\tilde{q}\}_n \tag{20}$$

where

$$[\tilde{k}] = \sum_{\text{Elements}} ([\Gamma_{\mathfrak{E}}]^t[\mathfrak{K}][\Gamma_{\mathfrak{E}}] + [\Gamma_{\mathfrak{E}}]^t[\mathfrak{R}][\Gamma_{\mathfrak{H}}]$$

$$+ [\Gamma_E]^t[K][\Gamma_E] + [\Gamma_E]^t[R][\Gamma_H] + [\Gamma_{\mathfrak{H}}]^t[\mathfrak{R}]^t[\Gamma_{\mathfrak{E}}] + [\Gamma_{\mathfrak{H}}]^t[\mathfrak{S}][\Gamma_{\mathfrak{X}}]$$

$$+ [\Gamma_H]^t[R]^t[\Gamma_E] + [\Gamma_H]^t[S][\Gamma_X] + [\Gamma_{\mathfrak{X}}]^t[\mathfrak{S}]^t[\Gamma_{\mathfrak{H}}] + [\Gamma_X]^t[S]^t[\Gamma_H]) \tag{21}$$

$$[\tilde{k}] = \sum_{\text{Elements}} ([\Gamma_{\mathfrak{E}}]^t[\bar{\mathfrak{K}}][\Gamma_{\mathfrak{E}}] + [\Gamma_E]^t[\bar{K}]^t[\Gamma_{\mathfrak{E}}]) \tag{22}$$

and

$$\{\tilde{q}\} = \sum_{\text{Elements}} ([\Gamma_{\mathfrak{X}}]^t\{\mathfrak{Q}\} + [\Gamma_X]^t\{Q\}) \tag{23}$$

In equations (21) to (23) the subscript n has been dropped for convenience.

Note that the chosen global approximation vectors (eqs. (17) to (19)) are the same as those used in the Taylor series expansion of the response in terms of λ. These vectors provide a direct measure of the sensitivity of the different response quantities to nonorthotropic (anisotropic) material stiffness coefficients of the tire. A comparison between the predictions of the foregoing technique and the Taylor series expansion is given in section 8.

5.4 Case of Axisymmetric Loading

If the Fourier harmonic n is set equal to zero in equations (7) to (10), the governing equations for the axisymmetric loading case are obtained. All the barred loading components and shell variables vanish, and the subvectors $\{\mathfrak{E}\}$, $\{E\}$, $\{\mathfrak{H}\}$, $\{H\}$, $\{\mathfrak{X}\}$, $\{X\}$, $\{\mathfrak{Q}\}$, and $\{Q\}$ are now associated with the fundamental unknowns (and external loadings), as shown in table 3.

The corresponding matrices in equations (13) and (14) have different dimensions. For $\lambda = 0$, the uncoupling of equations (13) and (14) signifies the uncoupling of the response of orthotropic (and isotropic) shells to normal and meridional loading from the response to circumferential loading. (See sections 2.1 and 2.4.)

6 NONLINEAR ANALYSIS OF ANISOTROPIC TIRES THROUGH USE OF TWO-DIMENSIONAL SHELL FINITE ELEMENTS

As a second application of the aforementioned computational strategy, consider the geometrically nonlinear analysis of anisotropic tires by use of three-field mixed two-dimensional shell finite elements. The material stiffness matrix of the

shell is decomposed into the sum of an orthotropic and a nonorthotropic (anisotropic) part, and the governing nonlinear finite-element equations for individual elements are embedded into a two-parameter family of equations of the form

$$\left(\begin{bmatrix} \bar{K} & R & 0 \\ R^t & 0 & S \\ 0 & S^t & 0 \end{bmatrix} + \lambda \begin{bmatrix} \bar{K} & 0 & 0 \\ 0 & 0 & 0 \\ 0 & 0 & 0 \end{bmatrix}\right) \begin{Bmatrix} E \\ H \\ X \end{Bmatrix} + \begin{Bmatrix} 0 \\ \mathfrak{G}(X) \\ \mathfrak{M}(H,X) \end{Bmatrix} - q \begin{Bmatrix} 0 \\ 0 \\ 0 \end{Bmatrix} = 0 \tag{24}$$

where $\{X\}$, $\{E\}$, and $\{H\}$ are the vectors of nodal displacements, strain parameters, and stress-resultant parameters; $\{\mathfrak{G}(X)\}$ and $\{\mathfrak{M}(H,X)\}$ are vectors of nonlinear contributions; $\{Q\}$ is the vector of normalized external loading coefficients; q is a loading parameter; and λ is a tracing parameter which identifies all the nonorthotropic (anisotropic) contributions to the element equations. The explicit forms of the arrays $[\bar{K}]$, $[\bar{K}]$, $[R]$, $[S]$, $\{\mathfrak{G}(X)\}$, $\{\mathfrak{M}(H,X)\}$, and $\{Q\}$ are given in appendix D.

With λ and q chosen as the control parameters, a two-parameter reduction method is applied to reduce both the size of the analysis model and the total number of degrees of freedom used in the initial discretization. This reduction is accomplished by use of the following transformation:

$$\begin{Bmatrix} E \\ H \\ X \end{Bmatrix} = \begin{bmatrix} \Gamma_E \\ \Gamma_H \\ \Gamma_X \end{bmatrix} \{\psi\} \tag{25}$$

where $\{\psi\}$ is a vector of amplitudes of global approximation vectors which are functions of both λ and q, and the $[\Gamma]$ terms are transformation matrices whose columns are the global approximation vectors consisting of the solution at $\lambda = q = 0$ and its various-order derivatives with respect to λ and q, that is,

$$[\Gamma_E] = \left[\{E\} \quad \left\{\frac{\partial E}{\partial q}\right\} \quad \left\{\frac{\partial E}{\partial \lambda}\right\} \quad \left\{\frac{\partial^2 E}{\partial q\, \partial \lambda}\right\} \quad \ldots\right] \tag{26}$$

$$[\Gamma_H] = \left[\{H\} \quad \left\{\frac{\partial H}{\partial q}\right\} \quad \left\{\frac{\partial H}{\partial \lambda}\right\} \quad \left\{\frac{\partial^2 H}{\partial q\, \partial \lambda}\right\} \quad \ldots\right] \tag{27}$$

$$[\Gamma_X] = \left[\{X\} \quad \left\{\frac{\partial X}{\partial q}\right\} \quad \left\{\frac{\partial X}{\partial \lambda}\right\} \quad \left\{\frac{\partial^2 X}{\partial q\, \partial \lambda}\right\} \quad \ldots\right] \tag{28}$$

The equations used in generating the global approximation vectors are obtained by successive differentiation with respect to q and λ of the finite-element equations of the discretized tire (eqs. (24)) and are listed in appendix E. For convenience, the initial set of global approximation vectors is generated at $\lambda = q = 0$. This reduces the computational effort in evaluating the global approximation vectors because of the following: for $q = 0$, $\{E\}$, $\{H\}$, and $\{X\}$ vanish, as do all the nonlinear terms on the left-hand sides of equations (E1); and for $\lambda = 0$, each of the global approximation vectors exhibits known types of symmetries (or antisymmetries) similar to those exhibited by the response of orthotropic tires, and therefore the size of the model used in generating these vectors is the same as that used for orthotropic tires.

The classic Rayleigh-Ritz technique is used to replace equations (24) with the following system of nonlinear equations in the unknown parameters $\{\psi\}$:

$$\left[[\tilde{k}] + \lambda[\tilde{k}]\right]\{\psi\} + \{\tilde{m}(\psi)\} - q\{\tilde{q}\} = 0 \tag{29}$$

where

$$[\tilde{k}] = \sum_{\text{Elements}} ([\Gamma_E]^t[\bar{K}][\Gamma_E] + [\Gamma_E]^t[R][\Gamma_H] + [\Gamma_H]^t[R]^t[\Gamma_E] + [\Gamma_H]^t[S][\Gamma_X] + [\Gamma_X]^t[S]^t[\Gamma_H]) \tag{30}$$

$$[\tilde{k}] = \sum_{\text{Elements}} [\Gamma_E]^t[\bar{K}][\Gamma_E] \tag{31}$$

$$\{\tilde{m}(\psi)\} = \sum_{\text{Elements}} ([\Gamma_H]^t\{\mathfrak{G}(\psi)\} + [\Gamma_X]^t\{\mathfrak{M}(\psi)\}) \tag{32}$$

and

$$\{\tilde{q}\} = \sum_{\text{Elements}} [\Gamma_X]^t\{Q\} \tag{33}$$

The nonlinear vectors $\{\mathfrak{G}(\psi)\}$ and $\{\mathfrak{M}(\psi)\}$ are obtained from the vectors $\{\mathfrak{G}(X)\}$ and $\{\mathfrak{M}(H,X)\}$ through replacement of $\{H\}$ and $\{X\}$ with their expressions in terms of $\{\psi\}$ (eqs. (25)).

7 NONLINEAR ANALYSIS OF ORTHOTROPIC TIRES SUBJECTED TO UNSYMMETRIC LOADING

As a final application of the computational strategy, consider the geometrically nonlinear analysis of orthotropic tires subjected to the localized loading shown in figure 5(b). The loading is unsymmetric with respect to reflection in the x-y plane, but it is symmetric with respect to reflections in the x-z and y-z planes. (See fig. 3.) The tire is modeled by use of three-field mixed two-dimensional shell elements. The loading vector is decomposed into symmetric and antisymmetric loadings (with respect to reflections in the x-y plane), and the governing nonlinear finite-element equations for individual elements are embedded in a two-parameter family of equations of the form

$$\begin{bmatrix} K & R & 0 \\ R^t & 0 & S \\ 0 & S^t & 0 \end{bmatrix} \begin{Bmatrix} E \\ H \\ X \end{Bmatrix} + \begin{Bmatrix} 0 \\ \mathfrak{G}(X) \\ \mathfrak{M}(H,X) \end{Bmatrix} - q_1 \begin{Bmatrix} 0 \\ 0 \\ Q_1 \end{Bmatrix} - q_2 \begin{Bmatrix} 0 \\ 0 \\ Q_2 \end{Bmatrix} = 0 \tag{34}$$

where q_1 and q_2 are normalized loading parameters and $\{Q_1\}$ and $\{Q_2\}$ are the vectors of normalized symmetric and antisymmetric loadings.

With q_1 and q_2 chosen as the control parameters, a two-parameter reduction method is applied to reduce both the size of the analysis model and the total number of degrees of freedom used in the initial discretization. This reduction

is accomplished with the procedure outlined in section 6. Note that the evaluation of the global approximation vectors at $q_1 = q_2 = 0$ allows the reduction of the size of the analysis model to just one octant of the tire (instead of the one quadrant required for the original unsymmetric loading). Each of the global approximation vectors exhibits known symmetry (or antisymmetry) along the centerlines.

The following observations can be made with regard to the proposed computational procedure:

1. Although the individual global approximation vectors exhibit symmetry (or antisymmetry) along their centerlines, their linear combination, which approximates the response to the general unsymmetric loading, is generally unsymmetric.

2. The reduced equations can be formed by use of only one octant of the tire. However, the solution of these equations approximates the unsymmetric response over one quadrant of the tire and consequently over the entire tire.

3. In case the given loading is antisymmetric (i.e., $q_1 = 0$), the procedure can be simplified, since only one parameter q is needed. Obviously, for symmetric loadings the response is symmetric.

4. Updated sets of global approximation vectors may be formed with the computational strategy, but it is essential that the tire configuration used in generating these vectors be symmetric (e.g., $q_2 = 0$).

8 NUMERICAL EXAMPLES

To evaluate the effectiveness of the proposed computational strategy, a number of quasi-symmetric tire problems have been analyzed. For each problem, the solutions obtained with the proposed strategy are compared with the direct analysis of the tire. The results of three typical problems are discussed herein. The three problems are linear response of an anisotropic tire subjected to normal pressure loading, linear response of an anisotropic tire subjected to uniform inflation pressure and localized loading, and geometrically nonlinear response of an orthotropic tire subjected to uniform inflation pressure and unsymmetric localized loading. The three problems correspond to the computational procedures presented in sections 5 to 7.

In the first problem, the tire is discretized with semianalytic finite elements (Fourier series expansions in the circumferential direction and finite elements in the meridional direction). In the last two problems, two-dimensional shell finite elements are used for the discretization. The tires are assumed to be rigidly clamped at the rim (at $\xi = \pm 1$), to have elliptic cross sections, and to be made of cord-rubber composite material. The geometric and material properties are given in figure 6. Small research-oriented programs were used to obtain all the numerical results presented herein.

8.1 Linear Response of an Anisotropic Tire Subjected to Normal Pressure Loading

The first problem considered is that of the linear response of an anisotropic tire subjected to normal pressure loading which is uniform in the meridional direction. Two loading cases are considered. The first is an axisymmetric loading

(inflation pressure) with $n = 0$, and the second is a nonaxisymmetric loading with $n = 2$. Since both the tire and the loading have axial symmetry as well as dihedral rotational symmetry, only half the meridian is analyzed. The symmetry conditions at $\xi = 0$ are $u = \phi_s = 0$ and $v = \bar{w} = \phi_\theta = 0$. Eight one-dimensional finite elements are used to obtain converged solution. Quadratic interpolation functions are used for approximating each of the stress resultants and strain components, and cubic interpolation functions are used for approximating each of the generalized displacements. The nonzero degrees of freedom consist of 118 generalized displacement coefficients, 192 stress parameters, and 192 strain parameters. Typical results are presented in figures 7 and 8 for $n = 0$ and in figure 9 for $n = 2$.

The proposed strategy is applied to this problem and the global approximation vectors are generated at $\lambda = 0$ and used to generate the solutions at $\lambda = 1$. The distribution of the first three nonzero global approximation vectors along the meridian for $n = 0$ is shown in figure 7. Note that the odd-order derivatives of $\{E\}$, $\{X\}$, and $\{H\}$ and the even-order derivatives of $\{E\}$, $\{X\}$, and $\{H\}$ with respect to λ are zero.

The even-order derivatives of u_0, w_0, $N_{\theta,0}$, and $M_{\theta,0}$ are shown in figure 7(a), and the odd-order derivatives of v_0, $\phi_{\theta,0}$, $N_{s\theta,0}$, and $M_{s\theta,0}$ are shown in figure 7(b). The magnitudes of the first-order and higher order derivatives of the different response quantities are an indication of the sensitivity of these response quantities to the anisotropic material coefficients.

The tire responses corresponding to $\lambda = 1$ and $\lambda = 0$ are shown in figure 8 for $n = 0$ and in figure 9 for $n = 2$, along with the predictions of the proposed strategy based on the use of four and six (or six and eight) global approximation vectors. The symmetric response quantities (with respect to $\theta = 0$) are shown in figures 8(a), 9(a), and 9(c), and the antisymmetric response quantities are shown in figures 8(b), 9(b), and 9(d). Note that for $n = 0$, all the antisymmetric response quantities corresponding to $\lambda = 0$ vanish.

As shown in figures 8 and 9, for both $n = 0$ and $n = 2$ the response of the two-layered tire is sensitive to the nonorthotropic stiffness coefficients identified by λ. As the number of layers increases, the response becomes less sensitive to λ.

An indication of the accuracy of the solutions obtained with the proposed strategy is given in figure 8 for $n = 0$ and in figure 9 for $n = 2$. The generalized displacements and stress resultants predicted with the proposed strategy through use of six vectors are highly accurate except for $N_{s\theta,2}$, for which eight vectors are needed. (See fig. 9(b).) The solutions obtained with eight vectors are almost indistinguishable from the direct finite-element solution.

The numerical values of the amplitudes of the global approximation vectors in the proposed strategy are given in table 4. The corresponding amplitudes of the same vectors in the Taylor series expansion are also given in table 4.

8.2 Linear Response of an Anisotropic Tire Subjected to Uniform Inflation Pressure and Localized Loading

The second problem considered is that of the linear response of the anisotropic tire shown in figure 6 when subjected to uniform inflation pressure and

localized loading (simulating the contact pressure). Typical numerical results are shown in figures 5(a), 10, and 11.

In figure 5(a) normalized contour plots are shown for the two displacement components v and w produced by the given loading. In figure 10, normalized contour plots are shown for the generalized displacements and their first four derivatives with respect to λ evaluated at $\lambda = 0$. Figure 11 shows the accuracy and convergence of the normal displacement at the center w_c and of the total strain energy U obtained with the proposed computational strategy.

As expected, the normal displacement w, the stress resultants N_s, N_θ, $N_{s\theta}$, M_s, M_θ, and $M_{s\theta}$, and the strain components ε_s, ε_θ, $2\varepsilon_{s\theta}$, κ_s, κ_θ, and $2\kappa_{s\theta}$ exhibit rotational (inversion) symmetry. The in-plane displacements u and v, the rotation components ϕ_s and ϕ_θ, the transverse-shear stress resultants Q_s and Q_θ, and the transverse-shear strains $2\varepsilon_{s3}$ and $2\varepsilon_{\theta 3}$ exhibit rotational (inversion) antisymmetry. These symmetry properties are used in conjunction with the procedure outlined in references 7 and 8 to reduce the analysis model to half the tire. (See fig. 5(a).) A uniform grid of two-dimensional elements is used. Biquadratic shape functions are used to approximate each of the generalized displacements, and bilinear shape functions are used to approximate each of the stress resultants and the strain components (a total of 717 nonzero displacement degrees of freedom, 1280 stress-resultant parameters, and 1280 strain parameters). The Gauss-Legendre quadrature formula with four quadrature points in the element domain is used for the evaluation of the elemental arrays. The highly anisotropic response of the tire is given in figure 5(a), in which normalized contour plots are shown for the v and w displacements.

The proposed strategy is applied to the analysis of the tire. Global approximation vectors are generated at $\lambda = 0$ and are used to generate the solution corresponding to $\lambda = 1$. The global approximation vectors exhibit reflection symmetry (or antisymmetry) with respect to $\xi = 0$ and $\theta = \pi$. These symmetry relations are shown in figure 10. They clearly demonstrate the fact that the global approximation vectors can each be obtained by analyzing only one quadrant of the tire.

An indication of the accuracy and convergence of the solutions obtained with the proposed strategy and with the Taylor series expansion is given in figure 11. The standard of comparison is taken to be the direct linear finite-element solution of the anisotropic tire with the technique described in references 8 and 9. As can be seen from figure 11, the solutions obtained with the proposed strategy are considerably more accurate than those obtained with the corresponding Taylor series expansions (based on the same global approximation vectors). As an example of this, the errors in the total strain energy obtained with the Taylor series with four and seven global approximation vectors are 16.3 percent and 5.25 percent. The corresponding errors in the strain energy obtained with the proposed strategy are only 0.15 percent and 0.001 percent.

8.3 Geometrically Nonlinear Response of an Orthotropic Tire Subjected to Uniform Inflation Pressure and Unsymmetric Localized Loading

The last problem considered is that of the geometrically nonlinear response of a tire subjected to uniform inflation pressure and localized loading which is

unsymmetric with respect to reflection in the x-y plane. (See fig. 3.) The maximum intensity of the localized loading is 8.662×10^5 Pa (125 psi). The material properties are given in figure 6, and to simplify the analysis, the anisotropic bending-extensional coupling coefficients of the tire are neglected (i.e., the tire is treated as orthotropic).

The unsymmetric localized loading is decomposed into symmetric and antisymmetric components, as shown in figure 12. The path parameters are selected to be the two loading parameters q_1 and q_2 associated with the symmetric and antisymmetric loading components. Only one quadrant of the tire is modeled with a uniform grid of two-dimensional elements (a total of 371 nonzero displacement degrees of freedom, 640 stress-resultant parameters, and 640 strain parameters). Ten global approximation vectors are generated at zero values of q_1 and q_2 (but at a uniform inflation pressure p_o of 6.895×10^5 Pa (100 psi)). The global approximation vectors include the axisymmetric nonlinear response ($\{E\}$, $\{H\}$, and $\{X\}$) evaluated at $p_o = 6.895 \times 10^5$ Pa and $q_1 = q_2 = 0$ and all its derivatives up to the fifth derivatives with respect to q_1 and q_2. These global approximation vectors and the reduced equations are generated through use of only one quadrant of the tire and the appropriate reflection symmetry and antisymmetry conditions. Normalized contour plots for the generalized displacements are given in figure 12. The reflection symmetry (or antisymmetry) for the solution at $q_1 = q_2 = 0$ and its first, second, and third derivatives with respect to $\xi = 0$ and $\theta = \pi/2$ is presented in figure 12. Since the major cost of the analysis is generating the global approximation vectors and the coefficients of the reduced equations, the proposed computational strategy enhances the efficiency of the reduction technique.

An indication of the accuracy and the convergence of the solutions obtained with the proposed strategy is given in table 5. The standard of comparison is taken to be the direct nonlinear finite-element solution of the orthotropic tire. As shown in table 5, the solutions obtained with the proposed strategy are highly accurate. The errors in the normal displacement w_c and in the total strain energy U obtained by use of six global approximation vectors (solution at $q_1 = q_2 = 0$ and all its first and second derivatives with respect to q_1 and q_2) are only 0.83 percent and 0.06 percent. These errors reduce further when more approximation vectors are used. (See table 5.)

9 POTENTIAL OF PROPOSED COMPUTATIONAL STRATEGY

The proposed strategy generates the solution of a complex tire problem (with anisotropic materials, unsymmetric imperfections, and unsymmetric loading) using small or *large perturbations* from the response of a simpler system (e.g., an orthotropic tire with no imperfections). The strategy has high potential for handling practical tire problems. In particular, the following observations and extensions of the strategy can be made.

1. The tire response, in both the proposed strategy and the Taylor series expansion of the response in terms of λ, is expressed as a linear combination of the same global approximation vectors. However, the coefficients of the linear combination in the Taylor series expansion are fixed and are equal to 1, λ, $\lambda^2/2!$, ..., $\lambda^{r-1}/(r-1)!$. By contrast, the coefficients in the proposed strategy are left as free parameters and are determined with the Rayleigh-Ritz technique. Numerical experiments have shown that the use of free parameters leads to accurate

solutions not only within the radius of convergence of the Taylor series but also well beyond it.

2. The proposed strategy can be used to analyze tires with unsymmetric imperfections. The unsymmetric imperfections are decomposed into symmetric and antisymmetric components. The terms in the governing finite-element equations (24) associated with the antisymmetric imperfections are grouped together and multiplied by the tracing parameter λ. The global approximation vectors are generated at $\lambda = 0$. The size of the analysis model used in generating these vectors is the same as that for a tire with symmetric imperfections.

3. The proposed strategy can be applied to contact problems of tires. The contact conditions can be treated as displacement-dependent unsymmetric boundary conditions. The unsymmetric response of the tire is approximated by a linear combination of symmetric and antisymmetric global approximation vectors (or modes). The governing nonlinear finite-element equations are restructured to delineate the contributions to the symmetric and antisymmetric responses. A tracing parameter λ is used to identify all the contributions to the antisymmetric response. The size of the analysis model used in generating the global approximation vectors is identical to that of the corresponding structure with symmetric contact conditions. The amplitudes of the global approximation vectors are obtained through solution of a reduced set of nonlinear equations corresponding to $\lambda = 1$.

4. The proposed strategy can be extended to tire problems with more than one source for the symmetry breaking through attachment of a tracing parameter with the terms in the governing finite-element equations associated with each source. However, as the number of independent tracing parameters increases, both the number of global approximation vectors that need to be generated and the size of the reduced system of equations increase at a faster rate. Therefore, for practical applications to tire problems, an attempt should be made to minimize the number of independent tracing parameters by treating some of the tracing parameters as functions of others.

5. In the application of the proposed strategy to tires subjected to unsymmetric loading, it is essential that the tire configuration used in generating the global approximation vectors be symmetric. This may limit the applicability of the strategy to cases in which the magnitudes of the unsymmetric loading components are not very large.

6. The proposed strategy can be applied to other mechanics problems. In particular, it can be used to generate the response of a complex structural system as a large perturbation from the response of a simpler system. It is also possible to use a hierarchy of simpler systems to generate the response of the complex structural system by choosing a number of tracing (or control) parameters and successively applying a single-parameter reduction method with each of the parameters.

10 CONCLUSIONS

Three basic types of symmetry (and their combinations) exhibited by tire response are identified. An efficient computational strategy is presented for reducing both the size of the model and the cost of the analysis of tires in the presence of symmetry-breaking conditions (e.g., unsymmetric material, geometry, or loading). The strategy is based on approximating the unsymmetric response of the tire by a linear combination of symmetric and antisymmetric global approximation vectors (or modes).

The three main elements of the computational strategy are the following: (1) use of three-field mixed models having independent shape functions for stress resultants, strain components, and generalized displacements, with the stress resultants and the strain components allowed to be discontinuous at interelement boundaries; (2) use of operator splitting (additive decomposition of some of the matrices and vectors used in the finite-element model) to delineate the symmetric and antisymmetric responses; and (3) successive use of the finite-element model and the classic Rayleigh-Ritz technique to substantially reduce the number of degrees of freedom. The finite-element method is first used to generate a few global approximation vectors (or modes). Then the amplitudes of these modes are computed through use of the Rayleigh-Ritz technique.

The proposed computational strategy was applied to the following three quasi-symmetric problems of tires:

1. Linear analysis of anisotropic tires (subjected to arbitrary loading) through use of semianalytic finite elements

2. Nonlinear analysis of anisotropic tires through use of two-dimensional shell finite elements

3. Nonlinear analysis of orthotropic tires subjected to unsymmetric loading

In the first two applications, the anisotropy (nonorthotropy) of the tire is the source of the symmetry breaking; in the third application, the quasi-symmetry is due to the unsymmetry of the loading.

The effectiveness of the proposed computational strategy is demonstrated with numerical examples, and its potential for handling practical tire problems is discussed. The results of the study suggest the following conclusions relative to the importance of the three main elements of the proposed computational strategy and to the potential of the proposed computational strategy:

1. The use of the three-field mixed models enhances the effectiveness of the proposed computational strategy and offers the following advantages over the equivalent displacement models:

A. To reduce the model size of anisotropic tires, the decomposition of the material stiffness matrix of the tire affects only the linear arrays $[K]$ and $[K]$ of the tire. By contrast, if a displacement model is used, both linear and nonlinear arrays are affected by the decomposition.

B. The generation of the global approximation vectors is easier and involves fewer arithmetic operations than in the displacement formulation. This is because the nonlinear terms of the mixed models are bilinear (or quadratic) in the nodal displacements and in the stress-resultant parameters and are not cubic as in the displacement formulation.

C. Experience with reduction methods based on mixed models and displacement formulations has demonstrated that, for a given number of global approximation vectors, the accuracy of the solutions obtained with the reduction method and mixed models is higher than that obtained with the corresponding reduction method and displacement models. This is particularly true for stress resultants and strain components.

2. The use of path derivatives as global approximation vectors leads to accurate solutions with a small number of vectors. Therefore, the time required to solve the reduced equations is relatively small, and the total analysis time to a first approximation equals the time required to evaluate the global approximation vectors and to generate the reduced equations. The operator splitting technique allows the reduction of the size of the analysis model of the tire and, therefore, the time needed to generate the global approximation vectors is reduced.

3. The global approximation vectors provide a direct measure of the sensitivity of the different response quantities to the tracing parameters used and their associated effects (e.g., anisotropic (nonorthotropic) material coefficients of the tire, geometric imperfections, or unsymmetric contact conditions). The sensitivity of the global response can also be assessed with these vectors.

4. The reduction method used in the proposed computational strategy exploits the best elements of the finite-element method and of the Rayleigh-Ritz technique, as follows:

A. The finite-element method is used as a general approach for generating global approximation vectors. The size of the analysis model used in generating these vectors is the same as that of the corresponding orthotropic panel.

B. The Rayleigh-Ritz technique is used as an efficient procedure for minimizing and distributing the error throughout the structure.

5. The reduction method extends the range of applicability of the Taylor series expansion by relaxing the requirement of using small loading and tracing parameters in the expansion.

NASA Langley Research Center
Hampton, VA 23665-5225
January 7, 1987

APPENDIX A - FUNDAMENTAL EQUATIONS OF SHELL THEORY USED IN THE PRESENT STUDY

The fundamental equations of the Sanders-Budiansky type shell of revolution used in the present study are summarized herein. The effects of laminated, anisotropic material response and transverse-shear deformation are included.

Strain Displacement Relationships

The relationships between the strains and generalized displacements of the middle surface are given by

$$\varepsilon_s = \partial_s u + \frac{w}{R_1} + \frac{1}{2}\left(\frac{u}{R_1} - \partial_s w\right)^2 + \frac{1}{2}\phi^2 \tag{A1}$$

$$\varepsilon_\theta = \frac{\partial_s r}{r} u + \frac{1}{r}\partial_\theta v + \frac{w}{R_2} + \frac{1}{2}\left(\frac{v}{R_2} - \frac{1}{r}\partial_\theta w\right)^2 + \frac{1}{2}\phi^2 \tag{A2}$$

$$2\varepsilon_{s\theta} = \frac{1}{r}\partial_\theta u + \left(\partial_s - \frac{\partial_s r}{r}\right) v + \left(\frac{u}{R_1} - \partial_s w\right)\left(\frac{v}{R_2} - \frac{1}{r}\partial_\theta w\right) \tag{A3}$$

$$\kappa_s = \partial_s \phi_s \tag{A4}$$

$$\kappa_\theta = \frac{\partial_s r}{r}\phi_s + \frac{1}{r}\partial_\theta \phi_\theta \tag{A5}$$

$$2\kappa_{s\theta} = \frac{1}{r}\partial_\theta \phi_s + \left(\partial_s - \frac{\partial_s r}{r}\right)\phi_\theta + \left(\frac{1}{R_2} - \frac{1}{R_1}\right)\phi \tag{A6}$$

$$2\varepsilon_{s3} = -\frac{u}{R_1} + \partial_s w + \phi_s \tag{A7}$$

$$2\varepsilon_{\theta 3} = -\frac{v}{R_2} + \frac{1}{r}\partial_\theta w + \phi_\theta \tag{A8}$$

where ε_s and ε_θ are the extensional strains in the meridional and circumferential directions, $2\varepsilon_{s\theta}$ is the in-plane shearing strain, κ_s and κ_θ are the bending strains in the meridional and circumferential directions, $2\kappa_{s\theta}$ is the twisting strain, $2\varepsilon_{s3}$ and $2\varepsilon_{\theta 3}$ are the transverse-shear strains, $\partial_s \equiv \partial/\partial s$, $\partial_\theta \equiv \partial/\partial\theta$, and ϕ is the rotation around the normal to the shell, which is given by

$$\phi = \frac{1}{2}\left[-\frac{1}{r}\partial_\theta u + \left(\partial_s + \frac{\partial_s r}{r}\right) v\right] \tag{A9}$$

The nonlinear terms which account for moderate rotations are underlined with dashes in equations (A1) to (A3).

Constitutive Relations

The shell is assumed to be made of a laminated, anisotropic, linearly elastic material. Every point of the shell is assumed to possess a single plane of elastic symmetry parallel to the middle surface. The relationships between the stress resultants and the strain measures of the shell are given by

$$\begin{Bmatrix} N_s \\ N_\theta \\ N_{s\theta} \\ \hline M_s \\ M_\theta \\ M_{s\theta} \\ \hline Q_s \\ Q_\theta \end{Bmatrix} = \left[\begin{array}{ccc:ccc:cc} c_{11} & c_{12} & \textcircled{c_{16}} & f_{11} & f_{12} & \textcircled{f_{16}} & \cdot & \cdot \\ & c_{22} & \textcircled{c_{26}} & f_{12} & f_{22} & \textcircled{f_{26}} & \cdot & \cdot \\ & & c_{66} & \textcircled{f_{16}} & \textcircled{f_{26}} & f_{66} & \cdot & \cdot \\ \hdashline & & & d_{11} & d_{12} & \textcircled{d_{16}} & \cdot & \cdot \\ \text{Symmetric} & & & & d_{22} & \textcircled{d_{26}} & \cdot & \cdot \\ & & & & & d_{66} & \cdot & \cdot \\ \hdashline & & & & & & c_{55} & \textcircled{c_{45}} \\ & & & & & & & c_{44} \end{array}\right] \begin{Bmatrix} \varepsilon_s \\ \varepsilon_\theta \\ 2\varepsilon_{s\theta} \\ \hline \kappa_s \\ \kappa_\theta \\ 2\kappa_{s\theta} \\ \hline 2\varepsilon_{s3} \\ 2\varepsilon_{\theta 3} \end{Bmatrix} \qquad \text{(A10)}$$

where c, f, and d are shell stiffness coefficients. The nonorthotropic (anisotropic) terms are circled and the dots refer to zero terms.

APPENDIX B - FORMULAS FOR THE COEFFICIENTS IN THE FINITE-ELEMENT EQUATIONS FOR SEMIANALYTIC INDIVIDUAL ELEMENTS

The explicit forms of the elemental arrays $[K]_n$, $[K]_n$, $[\bar{K}]_n$, $[R]_n$, $[R]_n$, $[S]_n$, $[S]_n$, $\{Q\}_n$, and $\{Q\}_n$, associated with the harmonic n are given in this appendix. For convenience, each of these arrays is partitioned into blocks corresponding to contributions from individual nodes, stress resultants, or strain approximation functions. The expressions of the typical partitions (or blocks) are given subsequently. Note that the order of the strain parameters in these partitions is ε_s, ε_θ, $2\varepsilon_{s\theta}$, κ_s, κ_θ, $2\kappa_{s\theta}$, $2\varepsilon_{s3}$, and $2\varepsilon_{\theta 3}$; the order of the stress-resultant parameters is N_s, N_θ, $N_{s\theta}$, M_s, M_θ, $M_{s\theta}$, Q_s, and Q_θ; and the order of the generalized displacement coefficients is u, v, w, ϕ_s, and ϕ_θ.

A typical ij partition of the elemental array $[K]_n$ is given by

$$\int_0^{\ell}\int_0^{2\pi} \bar{N}^i \bar{N}^j \left(\begin{bmatrix} c_{11} & c_{12} & \cdot & f_{11} & f_{12} & \cdot & \cdot & \cdot \\ & c_{22} & \cdot & f_{12} & f_{22} & \cdot & \cdot & \cdot \\ & & \cdot & \cdot & \cdot & \cdot & \cdot & \cdot \\ & & & d_{11} & d_{12} & \cdot & \cdot & \cdot \\ & \text{Symmetric} & & & d_{22} & \cdot & \cdot & \cdot \\ & & & & & \cdot & \cdot & \cdot \\ & & & & & & c_{55} & \cdot \\ & & & & & & & \cdot \end{bmatrix} \cos^2 n\theta \right.$$

$$\left. + \begin{bmatrix} \cdot & \cdot & \cdot & \cdot & \cdot & \cdot & \cdot & \cdot \\ & \cdot & \cdot & \cdot & \cdot & \cdot & \cdot & \cdot \\ & & c_{66} & \cdot & \cdot & f_{66} & \cdot & \cdot \\ & & & \cdot & \cdot & \cdot & \cdot & \cdot \\ & & & & \cdot & \cdot & \cdot & \cdot \\ & & & \text{Symmetric} & & & d_{66} & \cdot & \cdot \\ & & & & & & & \cdot & \cdot \\ & & & & & & & & c_{44} \end{bmatrix} \sin^2 n\theta \right) r \, d\theta \, ds \qquad \text{(B1)}$$

The dots in equations (B1) and succeeding equations refer to zero terms. The ij partition of the elemental array $[K]_n$ is given by equations (B1) after interchanging $\cos^2 n\theta$ and $\sin^2 n\theta$.

The ij partition of the elemental array $[\bar{K}]_n$ is given by

$$\int_0^{\ell}\int_0^{2\pi} \bar{N}^i\bar{N}^j \left(\begin{bmatrix} \cdot & \cdot & c_{16} & \cdot & \cdot & f_{16} & \cdot & \cdot \\ \cdot & \cdot & c_{26} & \cdot & \cdot & f_{26} & \cdot & \cdot \\ \cdot & \cdot & \cdot & \cdot & \cdot & \cdot & \cdot & \cdot \\ \cdot & \cdot & f_{16} & \cdot & \cdot & d_{16} & \cdot & \cdot \\ \cdot & \cdot & f_{26} & \cdot & \cdot & d_{26} & \cdot & \cdot \\ \cdot & \cdot & \cdot & \cdot & \cdot & \cdot & \cdot & \cdot \\ \cdot & \cdot & \cdot & \cdot & \cdot & \cdot & \cdot & c_{45} \\ \cdot & \cdot & \cdot & \cdot & \cdot & \cdot & \cdot & \cdot \end{bmatrix} \cos^2 n\theta \right.$$

$$\left. - \begin{bmatrix} \cdot & \cdot & \cdot & \cdot & \cdot & \cdot & \cdot & \cdot \\ \cdot & \cdot & \cdot & \cdot & \cdot & \cdot & \cdot & \cdot \\ c_{16} & c_{26} & \cdot & f_{16} & f_{26} & \cdot & \cdot & \cdot \\ \cdot & \cdot & \cdot & \cdot & \cdot & \cdot & \cdot & \cdot \\ \cdot & \cdot & \cdot & \cdot & \cdot & \cdot & \cdot & \cdot \\ f_{16} & f_{26} & \cdot & d_{16} & d_{26} & \cdot & \cdot & \cdot \\ \cdot & \cdot & \cdot & \cdot & \cdot & \cdot & \cdot & \cdot \\ \cdot & \cdot & \cdot & \cdot & \cdot & \cdot & c_{45} & \cdot \end{bmatrix} \sin^2 n\theta \right) r\, d\theta\, ds \qquad \text{(B2)}$$

The ij partition of the elemental array $[\bar{R}]_n$ can be written as the sum of two diagonal matrices as follows:

$$-\int_0^{\ell}\int_0^{2\pi} \bar{N}^i\bar{N}^j \left(\begin{bmatrix} 1 & & & & & \\ & 1 & & & & \\ & & \cdot & & & \\ & & & 1 & & \\ & & & & \cdot & \\ & & & & & 1 \\ & & & & & & \cdot \end{bmatrix} \cos^2 n\theta + \begin{bmatrix} \cdot & & & & & \\ & \cdot & & & & \\ & & 1 & & & \\ & & & \cdot & & \\ & & & & 1 & \\ & & & & & \cdot \\ & & & & & & 1 \end{bmatrix} \sin^2 n\theta \right) r\, d\theta\, ds \qquad \text{(B3)}$$

The ij partition of the array $[\bar{R}]_n$ is given by equations (B3) after interchanging $\cos^2 n\theta$ and $\sin^2 n\theta$.

The ij partition of the elemental array $[\bar{S}]_n$ is given by

$$\int_0^{\ell}\int_0^{2\pi} \bar{N}^i \left(\left[\begin{array}{ccc|cc} \partial_s N^j & \cdot & \frac{1}{R_1}N^j & \cdot & \cdot \\ \frac{\partial_s r}{r}N^j & \frac{n}{r}N^j & \frac{1}{R_2}N^j & \cdot & \cdot \\ \cdot & \cdot & \cdot & \cdot & \cdot \\ \hline \cdot & \cdot & \cdot & \partial_s N^j & \cdot \\ \cdot & \cdot & \cdot & \frac{\partial_s r}{r}N^j & \frac{n}{r}N^j \\ \cdot & \cdot & \cdot & \cdot & \cdot \\ \hline -\frac{N^j}{R_1} & \cdot & \partial_s N^j & N^j & \cdot \\ \cdot & \cdot & \cdot & \cdot & \cdot \end{array}\right] \cos^2 n\theta \right.$$

$$\left. + \left[\begin{array}{ccc|cc} \cdot & \cdot & \cdot & \cdot & \cdot \\ \cdot & \cdot & \cdot & \cdot & \cdot \\ \frac{n}{r}N^j & \frac{\partial_s r}{r}N^j - \partial_s N^j & \cdot & \cdot & \cdot \\ \hline \cdot & \cdot & \cdot & \cdot & \cdot \\ \cdot & \cdot & \cdot & \cdot & \cdot \\ \frac{n}{2r}\left(\frac{1}{R_1} - \frac{1}{R_2}\right)N^j & \frac{1}{2}\left(\frac{1}{R_1} - \frac{1}{R_2}\right)\left(\partial_s N^j + \frac{\partial_s r}{r}N^j\right) & \cdot & \frac{n}{r}N^j & \frac{\partial_s r}{r}N^j - \partial_s N^j \\ \hline \cdot & \cdot & \cdot & \cdot & \cdot \\ \cdot & \frac{1}{R_2}N^j & \frac{n}{r}N^j & \cdot & -N^j \end{array}\right] \sin^2 n\theta \right) r\, d\theta\, ds \qquad \text{(B4)}$$

The ij partition of the elemental array $[S]_n$ is given by equations (B4) after interchanging $\cos^2 n\theta$ and $\sin^2 n\theta$.

The ith partition of the array $\{Q\}_n$ is given by:

$$\int_0^{\ell} \int_0^{2\pi} N^i N^j \begin{Bmatrix} p^j_{s,n} \cos^2 n\theta \\ \bar{p}^j_{\theta,n} \sin^2 n\theta \\ p^j_n \cos^2 n\theta \\ m^j_{s,n} \cos^2 n\theta \\ \bar{m}^j_{\theta,n} \sin^2 n\theta \end{Bmatrix} r \, d\theta \, ds \tag{B5}$$

The ith partition of the array $\{Q\}_n$ is given by equation (B5) after interchanging $\cos^2 n\theta$ and $\sin^2 n\theta$.

In equations (B1) to (B5), ℓ is the length of the element; $\bar{N}^i$ and $\bar{N}^j$ are the shape functions for both the strain components and the stress resultants; N^j are the shape functions for the generalized displacements; c, f, and d are shell stiffnesses; r is the normal distance from the tire axis to the reference surface (see fig. 1); R_1 and R_2 are principal radii of curvature in the meridional and circumferential directions; s and θ are the meridional and circumferential coordinates of the shell; and $\partial_s \equiv \partial/\partial s$.

APPENDIX C - EVALUATION OF GLOBAL APPROXIMATION VECTORS BASED ON SEMIANALYTIC FINITE ELEMENTS

The global approximation vectors are chosen to be the solutions of equations (7) and (8), $\{\mathfrak{E}\}_n$, $\{\mathfrak{H}\}_n$, $\{\mathfrak{X}\}_n$, $\{E\}_n$, $\{H\}_n$, $\{X\}_n$, and their various-order path derivatives (derivatives of these solutions with respect to λ) evaluated at $\lambda = 0$. For $\lambda = 0$, equations (7) and (8) are uncoupled. The path derivatives are obtained by successive differentiation of the governing finite-element equations (7) and (8) with respect to λ and solution of the resulting two sets of uncoupled equations corresponding to $\lambda = 0$. For the individual finite elements, the recursion formulas for the path derivatives can be written in the following compact form:

$$\begin{bmatrix} \mathfrak{K} & \mathfrak{R} & 0 \\ \mathfrak{R}^t & 0 & \mathfrak{S} \\ 0 & \mathfrak{S}^t & 0 \end{bmatrix}_n \frac{\partial^m}{\partial\lambda^m} \begin{Bmatrix} \mathfrak{E} \\ \mathfrak{H} \\ \mathfrak{X} \end{Bmatrix}_n = \begin{Bmatrix} \mathfrak{P} \\ 0 \\ 0 \end{Bmatrix}_n \tag{C1}$$

and

$$\begin{bmatrix} K & R & 0 \\ R^t & 0 & S \\ 0 & S^t & 0 \end{bmatrix}_n \frac{\partial^m}{\partial\lambda^m} \begin{Bmatrix} E \\ H \\ X \end{Bmatrix}_n = \begin{Bmatrix} P \\ 0 \\ 0 \end{Bmatrix}_n \tag{C2}$$

where $m \geq 1$ and the vectors $\{\mathfrak{P}\}_n$ and $\{P\}_n$ on the right-hand sides of equations (C1) and (C2) are given by

$$\{\mathfrak{P}\}_n = -m \left[\bar{\mathfrak{K}}\right]_n \frac{\partial^{m-1}}{\partial\lambda^{m-1}} \{E\}_n \tag{C3}$$

and

$$\{P\}_n = -m \left[\bar{\mathfrak{K}}\right]_n^t \frac{\partial^{m-1}}{\partial\lambda^{m-1}} \{\mathfrak{E}\}_n \tag{C4}$$

Note that equations (C1) and (C2) are uncoupled and that the coefficient matrices on the left-hand sides of these equations, which must be factored for each Fourier harmonic n, are the same for all the path derivatives.

APPENDIX D - FORMULAS FOR THE COEFFICIENTS IN THE GOVERNING NONLINEAR EQUATIONS FOR INDIVIDUAL TWO-DIMENSIONAL SHELL FINITE ELEMENTS

The explicit forms of the arrays $[\bar{K}]$, $[R]$, $[S]$, $[\bar{K}]$, $\{\mathfrak{G}(X)\}$, $\{\mathfrak{M}(H,X)\}$, and $\{Q\}$ are given in this appendix. For convenience, each of these arrays is partitioned into blocks corresponding to contributions from individual nodes, strain, or stress-resultant approximation functions. The expressions of the typical partitions (or blocks) are given in table D1. Note that the order of the strain components in these partitions is ε_s, ε_θ, $2\varepsilon_{s\theta}$, κ_s, κ_θ, $2\kappa_{s\theta}$, $2\varepsilon_{s3}$, and $2\varepsilon_{\theta 3}$. The order of the stress resultants is N_s, N_θ, $N_{s\theta}$, M_s, M_θ, $M_{s\theta}$, Q_s, and Q_θ. The order of the nodal displacement parameters is u, v, w, ϕ_s, and ϕ_θ.

In table D1, $\bar{N}^{\mathcal{i}}$ and $\bar{N}^{\mathcal{j}}$ are the shape functions for both the stress resultants and strain components; N^j are the shape functions for the generalized displacements; r is the radial coordinate; m is the number of displacement nodes in the element; $[I]$ is the identity matrix; δ is the number of parameters used in approximating each of the stress resultants and strain components; $S^{(e)}$ is the element domain; $\partial_s \equiv \partial/\partial s$; and $\partial_\theta \equiv \partial/\partial\theta$. The range of the indices $\mathcal{i}$ and $\mathcal{j}$ is 1 to δ, and the range of the indices i and j is 1 to m. The dots in the matrices refer to zero terms. The quantities $\bar{\varepsilon}_1$ and $\bar{\varepsilon}_2$ are defined in terms of the displacement components as follows:

$$\bar{\varepsilon}_1 = \frac{u}{R_1} - \partial_s w$$

$$\bar{\varepsilon}_2 = \frac{v}{R_2} - \frac{1}{r}\partial_\theta w$$

Table D1.- Explicit Form of Typical Partitions of the Arrays $[\bar{K}]$, $[\bar{K}]$, $[R]$, $[S]$, $\{Q\}$, $\{\mathfrak{G}(X)\}$, and $\{\mathfrak{M}(H,X)\}$

Array	Number of partitions (or blocks)	Typical partition
$[\bar{K}]_{ij}$	$s \times s$	$\int_{S(e)} \bar{N}^i \bar{N}^j$ $\begin{bmatrix} c_{11} & c_{12} & \cdot & f_{11} & f_{12} & \cdot & \cdot & \cdot \\ & c_{22} & \cdot & f_{12} & f_{22} & \cdot & \cdot & \cdot \\ & & c_{66} & \cdot & \cdot & f_{66} & \cdot & \cdot \\ & & & d_{11} & d_{12} & \cdot & \cdot & \cdot \\ & & & & d_{22} & \cdot & \cdot & \cdot \\ \text{Symmetric} & & & & & d_{66} & \cdot & \cdot \\ & & & & & & c_{55} & \cdot \\ & & & & & & & c_{44} \end{bmatrix}$ $r\, d\theta\, ds$
$[\bar{K}]_{ij}$	$s \times s$	$\int_{S(e)} \bar{N}^i \bar{N}^j$ $\begin{bmatrix} \cdot & \cdot & c_{16} & \cdot & \cdot & f_{16} & \cdot & \cdot \\ & \cdot & c_{26} & \cdot & \cdot & f_{26} & \cdot & \cdot \\ & & \cdot & f_{16} & f_{26} & \cdot & \cdot & \cdot \\ & & & \cdot & \cdot & d_{16} & \cdot & \cdot \\ \text{Symmetric} & & & & \cdot & d_{26} & \cdot & \cdot \\ & & & & & \cdot & \cdot & \cdot \\ & & & & & & \cdot & c_{45} \\ & & & & & & & \cdot \end{bmatrix}$ $r\, d\theta\, ds$
$[R]_{ij}$	$s \times s$	$-\int_{S(e)} \bar{N}^i \bar{N}^j\, [I]_{8,8}\, r\, d\theta\, ds$

Table D1.- Continued

Array	Number of partitions (or blocks)	Typical partition
$[S]_{ij}$	$s \times m$	$\int_{S(e)} \bar{N}^i \begin{bmatrix} \partial_s & . & \frac{1}{R_1} & . & . \\ \frac{\partial_s r}{r} & \frac{1}{r}\partial_\theta & \frac{1}{R_2} & . & . \\ \frac{1}{r}\partial_\theta & \partial_s - \frac{\partial_s r}{r} & . & . & . \\ . & . & . & \partial_s & . \\ . & . & . & \frac{\partial_s r}{r} & \frac{1}{r}\partial_\theta \\ \frac{1}{2r}\left(\frac{1}{R_1} - \frac{1}{R_2}\right)\partial_\theta & -\frac{1}{2}\left(\frac{1}{R_1} - \frac{1}{R_2}\right)\left(\partial_s + \frac{\partial_s r}{r}\right) & . & \frac{1}{r}\partial_\theta & \partial_s - \frac{\partial_s r}{r} \\ -\frac{1}{R_1} & . & \partial_s & 1 & . \\ . & -\frac{1}{R_2} & \frac{1}{r}\partial_\theta & . & 1 \end{bmatrix} N^j r \, d\theta \, ds$
$\{Q\}_j$	m	$\int_{S(e)} N^j \begin{Bmatrix} p_s \\ p_\theta \\ p \\ m_s \\ m_\theta \end{Bmatrix} r \, d\theta \, ds$

Table D1.- Concluded

Array	Number of partitions (or blocks)	Typical partition
$\{\mathfrak{C}(X)\}_i$	s	$\int_{S(e)} \bar{N}^i \begin{Bmatrix} \frac{1}{2}\left(\frac{u}{R_1} - \partial_s w\right)^2 + \frac{1}{2}\phi^2 \\ \frac{1}{2}\left(\frac{v}{R_2} - \frac{1}{r}\partial_\theta w\right)^2 + \frac{1}{2}\phi^2 \\ \left(\frac{u}{R_1} - \partial_s w\right)\left(\frac{v}{R_2} - \frac{1}{r}\partial_\theta w\right) \\ \vdots \end{Bmatrix} r\, d\theta\, ds$
$\{\mathfrak{M}(H,X)\}_j$	m	$\int_{S(e)} \begin{Bmatrix} \frac{1}{R_1}(N_s\bar{\varepsilon}_1 + N_{s\theta}\bar{\varepsilon}_2) - \frac{1}{2r}(N_s + N_\theta)\phi\partial_\theta \\ \frac{1}{R_2}(N_{s\theta}\bar{\varepsilon}_1 + N_\theta\bar{\varepsilon}_2) + \frac{1}{2}(N_s + N_\theta)\phi\left(\partial_s + \frac{\partial_s r}{r}\right) \\ -(N_s\bar{\varepsilon}_1 + N_{s\theta}\bar{\varepsilon}_2)\partial_s - \frac{1}{r}(N_{s\theta}\bar{\varepsilon}_1 + N_\theta\bar{\varepsilon}_2)\partial_\theta \\ \vdots \end{Bmatrix} N^j r\, d\theta\, ds$

APPENDIX E - EVALUATION OF GLOBAL APPROXIMATION VECTORS BASED ON TWO-DIMENSIONAL SHELL FINITE ELEMENTS

The global approximation vectors in equations (26) to (28) are obtained by successive differentiation of the governing finite-element equations (24), with respect to the two parameters q and λ, and solution of the resulting system of linear simultaneous algebraic equations. For individual finite elements, the recursion formulas for the global approximation vectors can be written in the following compact form:

$$\begin{bmatrix} \bar{K} & R & 0 \\ & 0 & S + \dfrac{\partial \mathfrak{G}_I}{\partial X_J} \\ \text{Symmetric} & & \dfrac{\partial \mathfrak{M}_I}{\partial X_J} \end{bmatrix} \frac{\partial^{m+n}}{\partial q^m \, \partial \lambda^n} \begin{Bmatrix} E \\ H \\ X \end{Bmatrix} = - \begin{Bmatrix} \mathfrak{P}^{(m+n)} \\ \mathfrak{Q}^{(m+n)} \\ \mathfrak{R}^{(m+n)} \end{Bmatrix} \tag{E1}$$

where the range of I is 1 to 8δ (δ is the number of parameters used in approximating each of the stress resultants or strain components) and the range of I and J is 1 to $5m$ (m is the number of displacement nodes). The total number of $(m + n)$ combinations is $r - 1$, where r is the number of approximation vectors. The explicit forms of the first few values of $\{\mathfrak{P}^{(m+n)}\}$, $\{\mathfrak{Q}^{(m+n)}\}$, $\{\mathfrak{R}^{(m+n)}\}$ are given in table E1.

In table E1, a dot ($\cdot$) over a symbol refers to a derivative with respect to q and a prime ($'$) over a symbol refers to a derivative with respect to λ. Note that the coefficient matrix on the left-hand side of equations (E1), which must be factored, is the same for each of the global approximation vectors. Hence, this matrix is factored only once regardless of the number of global approximation vectors generated. If the global approximation vectors are generated at $\lambda = q = 0$, then $\{E\} = 0$, $\{H\} = 0$, and $\{X\} = 0$. Also, all the derivatives $\dfrac{\partial^n}{\partial \lambda^n}\{E\}$, $\dfrac{\partial^n}{\partial \lambda^n}\{H\}$, and $\dfrac{\partial^n}{\partial \lambda^n}\{X\}$ vanish, and equations (E1) are thus simplified. The computational effort in evaluating the global approximation vectors is thereby reduced.

Table E1.- First Explicit Forms of $\{\mathcal{P}^{(m+n)}\}$, $\{\mathcal{Q}^{(m+n)}\}$, and $\{\mathcal{R}^{(m+n)}\}$

$m+n$	m	n	$\{\mathcal{P}^{(m+n)}\}$	$\{\mathcal{Q}^{(m+n)}\}$	$\{\mathcal{R}^{(m+n)}\}$
1	1	0	0	0	$\{Q\}$
	0	1	$[K]\{E\}$	0	0
2	2	0	0	$\left\{\frac{\partial^2 \mathcal{G}_I}{\partial X_J\, \partial X_K}\, \dot{X}_J \dot{X}_K\right\}$	$2\left\{\frac{\partial^2 \mathcal{M}_I}{\partial H_J\, \partial X_K}\, \dot{H}_J \dot{X}_K\right\}$
	1	1	$[K]\{\dot{E}\}$	$\left\{\frac{\partial^2 \mathcal{G}_I}{\partial X_J\, \partial X_K}\, \dot{X}_J \acute{X}_K\right\}$	$\left\{\frac{\partial^2 \mathcal{M}_I}{\partial H_J\, \partial X_K}(\acute{H}_J \dot{X}_K + \dot{H}_J \acute{X}_K)\right\}$
	0	2	$2[K]\{\acute{E}\}$	$\left\{\frac{\partial^2 \mathcal{G}_I}{\partial X_J\, \partial X_K}\, \acute{X}_J \acute{X}_K\right\}$	$2\left\{\frac{\partial^2 \mathcal{M}_I}{\partial H_J\, \partial X_K}\, \acute{H}_J \acute{X}_K\right\}$
3	3	0	0	$3\left\{\frac{\partial^2 \mathcal{G}_I}{\partial X_J\, \partial X_K}\, \ddot{X}_J \dot{X}_K\right\}$	$3\left\{\frac{\partial^2 \mathcal{M}_I}{\partial H_J\, \partial X_K}(\dot{H}_J \ddot{X}_K + \ddot{H}_J \dot{X}_K)\right\}$
	2	1	$[K]\{\ddot{E}\}$	$\left\{\frac{\partial^2 \mathcal{G}_I}{\partial X_J\, \partial X_K}(\ddot{X}_J \acute{X}_K + 2\dot{X}_J \dot{X}_K)\right\}$	$\left\{\frac{\partial^2 \mathcal{M}_I}{\partial H_J\, \partial X_K}(\acute{H}_J \ddot{X}_K + 2\dot{H}_J \dot{X}_K + 2\dot{H}_J \acute{X}_K + \ddot{H}_J \acute{X}_K)\right\}$
	1	2	$2[K]\{\dot{\acute{E}}\}$	$\left\{\frac{\partial^2 \mathcal{G}_I}{\partial X_J\, \partial X_K}(\acute{\ddot{X}}_J \dot{X}_K + 2\dot{\acute{X}}_J \acute{X}_K)\right\}$	$\left\{\frac{\partial^2 \mathcal{M}_I}{\partial H_J\, \partial X_K}(\dot{H}_J \acute{\ddot{X}}_K + 2\dot{\acute{H}}_J \acute{X}_K + \acute{\ddot{H}}_J \dot{X}_K)\right\}$
	0	3	$3[K]\{\acute{\ddot{E}}\}$	$3\left\{\frac{\partial^2 \mathcal{G}_I}{\partial X_J\, \partial X_K}\, \acute{\ddot{X}}_J \acute{X}_K\right\}$	$3\left\{\frac{\partial^2 \mathcal{M}_I}{\partial H_J\, \partial X_K}(\acute{H}_J \acute{\ddot{X}}_K + \acute{\ddot{H}}_J \acute{X}_K)\right\}$

REFERENCES

1. Clark, Samuel K., ed.: Mechanics of Pneumatic Tires. U.S. Dep. Transp., 1981.

2. Tanner, John A., compiler: Tire Modeling. NASA CP-2264, 1983.

3. Noor, Ahmed K.; and Tanner, John A.: Advances and Trends in the Development of Computational Models for Tires. Comput. & Struct., vol. 20, no. 1-3, 1985, pp. 517-533.

4. Noor, Ahmed K.; and Peters, Jeanne M.: Mixed Models and Reduced Selective Integration Displacement Models for Vibration Analysis of Shells. Hybrid and Mixed Finite Element Methods, S. N. Atluri, R. H. Gallagher, and O. C. Zienkiewicz, eds., John Wiley & Sons Ltd., c.1983, pp. 537-564.

5. Wempner, G.; Talaslidis, D.; and Hwang, C.: A Simple and Efficient Approximation of Shells via Finite Quadrilateral Elements. J. Appl. Mech., vol. 49, no. 1, Mar. 1982, pp. 115-120.

6. Schaeffer, Harry G.; and Ball, Robert E.: Nonlinear Deflections of Asymmetrically Loaded Shells of Revolution. AIAA Paper No. 68-292, Apr. 1968.

7. Wunderlich, W.; Cramer, H.; and Obrecht, H.: Application of Ring Elements in the Nonlinear Analysis of Shells of Revolution Under Nonaxisymmetric Loading. Comput. Methods Appl. Mech. & Eng., vol. 51, nos. 1-3, Sept. 1985, pp. 259-275.

8. Noor, Ahmed K.; and Camin, Robert A.: Symmetry Considerations for Anisotropic Shells. Comput. Methods Appl. Mech. & Eng., vol. 9, no. 3, Nov.-Dec. 1976, pp. 317-335.

9. Noor, Ahmed K.; Mathers, Michael D.; and Anderson, Melvin S.: Exploiting Symmetries for Efficient Postbuckling Analysis of Composite Plates. AIAA J., vol. 15, no. 1, Jan. 1977, pp. 24-32.

10. Noor, Ahmed K.; and Peters, Jeanne M.: Reduced Basis Technique for Nonlinear Analysis of Structures. AIAA J., vol. 18, no. 4, Apr. 1980, pp. 455-462.

11. Noor, Ahmed K.: On Making Large Nonlinear Problems Small. Comput. Methods Appl. Mech. & Eng., vol. 34, nos. 1-3, Sept. 1982, pp. 955-985.

12. Noor, Ahmed K.; and Peters, Jeanne M.: Recent Advances in Reduction Methods for Instability Analysis of Structures. Comput. & Struct., vol. 16, no. 1-4, 1983, pp. 67-80.

13. Noor, Ahmed K.; Balch, Chad D.; and Shibut, Macon A.: Reduction Methods for Nonlinear Steady-State Thermal Analysis. Int. J. Numer. Methods Eng., vol. 20, no. 7, July 1984, pp. 1323-1348.

14. Noor, Ahmed K.; and Peters, Jeanne M.: Model-Size Reduction Technique for the Analysis of Symmetric Anisotropic Structures. Eng. Comput., vol. 2, no. 4, Dec. 1985, pp. 285-292.

15. Noor, Ahmed K.: Reduction Method for the Non-Linear Analysis of Symmetric Anisotropic Panels. Int. J. Numer. Methods Eng., vol. 23, 1986, pp. 1329-1341.

16. Noor, Ahmed K.; and Peters, Jeanne M.: Nonlinear Analysis of Anisotropic Panels. AIAA J., vol. 24, no. 9, Sept. 1986, pp. 1545-1553.

17. Sanders, J. Lyell, Jr.: Nonlinear Theories for Thin Shells. Q. Appl. Math., vol. XXI, no. 1, Apr. 1963, pp. 21-36.

18. Budiansky, Bernard: Notes on Nonlinear Shell Theory. Trans. ASME, Ser. E: J. Appl. Mech., vol. 35, no. 2, June 1968, pp. 393-401.

19. Glockner, Peter G.: Symmetry in Structural Mechanics. J. Struct. Div., American Soc. Civil Eng., vol. 99, no. ST1, Jan. 1973, pp. 71-89.

20. Hamermesh, Morton: Group Theory and Its Application to Physical Problems. Addison-Wesley Publ. Co., Inc., c.1962.

21. Dong, Richard G.; and Dong, Stanley B.: Analysis of Slightly Anisotropic Shells. AIAA J., vol. 1, no. 11, Nov. 1963, pp. 2565-2569.

22. Sarkisian, V. S.: Some Problems of Mathematical Elasticity Theory for Anisotropic Bodies. Yerevan, Izdatel'stvo Erevanskogo Universiteta, 1976.

23. Gould, Phillip L.: Finite Element Analysis of Shells of Revolution. Pitman Publ. Inc., c.1985.

24. Noor, Ahmed K.; and Andersen, C. M.: Mixed Models and Reduced/Selective Integration Displacement Models for Nonlinear Shell Analysis. Int. J. Numer. Methods Eng., vol. 18, no. 10, Oct. 1982, pp. 1429-1454.

SYMBOLS

a	radial distance for toroidal shell (see fig. 6)
b_o, b_1, b_2	parameters defining the elliptic profile of the tire cross section (see fig. 6)
c_{ij}, d_{ij}, f_{ij}	shell stiffness coefficients (i,j = 1,2,6)
c_{44}, c_{45}, c_{55}	transverse-shear stiffness coefficients of the shell
E_L, E_T	elastic moduli of the individual layers in the direction of fibers and normal to it
$\{E\}$	vector of strain parameters for a shell element (see eqs. (11) and (24))
$\{\mathfrak{E}\}, \{E\}$	vectors of strain parameters for a one-dimensional shell element (see eqs. (13) and (14))
G_{LT}, G_{TT}	shear moduli in plane of fibers and normal to it
$\{\mathfrak{G}(X)\}$, $\{\mathfrak{M}(H,X)\}$	vectors of nonlinear terms for a two-dimensional shell element (see eqs. (24))
$\{H\}$	vector of stress-resultant parameters (see eqs. (11) and (24))
$\{\mathfrak{H}\}, \{H\}$	vectors of stress-resultant parameters for a one-dimensional shell element (see eqs. (13) and (14))
h	total thickness of the shell
$[K], [\mathfrak{K}], [\underline{K}]$, $[\bar{K}], [\bar{\mathfrak{K}}], [\bar{\underline{K}}]$	elemental matrices (see eqs. (11), (13), (14), and (24))
$[\tilde{\mathfrak{k}}], [\tilde{k}]$	linear stiffness matrices of the reduced system (see eqs. (21), (22), (30), and (31))
$M_s, M_\theta, M_{s\theta}$	bending (and twisting) stress resultants (see fig. 2)
m	number of displacement nodes in the element
m_s, m_θ	intensity of external moments in the meridional and circumferential directions
$\{\tilde{m}(\psi)\}$	vector of nonlinear terms in the reduced system (see eqs. (32))
$N_s, N_\theta, N_{s\theta}$	extensional stress resultants (see fig. 2)
N	shape functions used for approximating the generalized displacements
$\bar{N}$	shape functions used for approximating the stress resultants and strain components
n	Fourier harmonic in the circumferential direction

p_o	intensity of normal pressure loading
p_s, p_θ, p	intensity of external loading in the coordinate directions (see fig. 2)
$\{Q\}, \{Q_1\}, \{Q_2\}$	vectors of normalized external loadings for individual elements (see eqs. (24) and (34))
Q_s, Q_θ	transverse-shear stress resultants (see fig. 2)
$\{\mathfrak{Q}\}, \{Q\}$	vectors of consistent external loadings and moment coefficients for a one-dimensional shell element (see eqs. (13) and (14))
q, q_1, q_2	loading parameters
$\{\tilde{q}\}$	loading vector of the reduced system (see eqs. (23) and (29))
R_1, R_2	principal radii of curvature in the meridional and circumferential directions
$[R], [\mathfrak{R}], [\mathcal{R}]$	linear matrices of the shell element (see eqs. (11), (13), (14), and (24))
r	normal distance from the shell axis to the reference surface
$\mathcal{r}$	number of global approximation vectors
$[S], [\mathfrak{S}], [\mathcal{S}]$	linear strain-displacement matrices of the shell element (see eqs. (11), (13), (14), and (24))
s	meridional coordinate of the shell (see fig. 2)
$\mathcal{s}$	number of parameters used in approximating each of the stress resultants and strain components within the individual elements
U	total strain energy of the shell
u,v,w	displacement components of the middle surface of the shell in the meridional, circumferential, and normal directions
w_c	normal displacement at the center
$\{X\}$	vector of nodal displacements
$\{\mathfrak{X}\}, \{X\}$	vectors of generalized nodal displacement coefficients for a one-dimensional shell element
x,y,z	Cartesian coordinate system (see fig. 3)
x_3	coordinate normal to the shell middle surface

$[\Gamma_E],[\Gamma_H],[\Gamma_X]$, $[\Gamma_{\mathfrak{E}}],[\Gamma_{\mathfrak{H}}],[\Gamma_{\mathfrak{X}}]$, $[\Gamma_E],[\Gamma_H],[\Gamma_X]$ — matrices of global approximation vectors defined in equations (16), (17), (18), (19), (26), (27), and (28)

$\varepsilon_s,\varepsilon_\theta,2\varepsilon_{s\theta}$ — extensional strains of the middle surface of the shell

$2\varepsilon_{s3},2\varepsilon_{\theta 3}$ — transverse-shear strains of the shell

θ — circumferential (hoop) coordinate of the shell (see fig. 2)

$\kappa_s,\kappa_\theta,2\kappa_{s\theta}$ — bending strains of the shell

λ — tracing parameter identifying all the anisotropic terms in the governing finite-element equations (see eqs. (13), (14), and (24))

ν_{LT} — major Poisson's ratio of the individual layers

ξ — dimensionless coordinate along the meridian (see fig. 3)

ϕ — rotation around the normal to the shell middle surface

ϕ_s,ϕ_θ — rotation components of the middle surface of the shell (see fig. 2)

$\{\psi\}$ — vector of amplitudes of global approximation vectors

∂_s — $\equiv \partial/\partial s$

∂_θ — $\equiv \partial/\partial\theta$

Ranges of indices:

$\mathcal{I},\mathcal{J}$ — 1 to 8δ

I,J — 1 to 5m

$\mathcal{i},\mathcal{j}$ — 1 to δ

i,j — 1 to m

Superscript t denotes transposition; subscript n refers to the nth Fourier harmonic.

Table 1.- Symmetry Conditions for Tires Exhibiting Rotational and/or Reflection Symmetry in Addition to Axial Symmetry

[See fig. 3]

Additional symmetries of tire and loading	Tire type	Symmetry conditions
Rotational symmetry about an axis normal to the axis of revolution (e.g., z-axis)	Orthotropic or anisotropic	At $\xi = 0$: $u = v = \phi_s = \phi_\theta = 0$ $Q_s = Q_\theta = 0$ $2\varepsilon_{s3} = 2\varepsilon_{\theta 3} = 0$
Reflection (or mirror) symmetry with respect to x-z plane	Orthotropic	At $\xi = 0$: $u = \phi_s = 0$ $N_{s\theta} = M_{s\theta} = Q_s = 0$ $2\varepsilon_{s\theta} = 2\kappa_{s\theta} = 2\varepsilon_{s3} = 0$
Rotational symmetry about axis normal to axis of revolution *and* reflection symmetry with respect to x-z plane	Orthotropic	At $-1 \leq \xi \leq 1$: $v = \phi_\theta = 0$ $N_{s\theta} = M_{s\theta} = Q_\theta = 0$ $2\varepsilon_{s\theta} = 2\kappa_{s\theta} = 2\varepsilon_{\theta 3} = 0$ At $\xi = 0$: $u = \phi_s = 0$ $Q_s = 0$ $2\varepsilon_{s3} = 0$

Table 2.- Symmetric and Antisymmetric Shell Variables

[Symmetric or antisymmetric with respect to $\theta = 0$]

Vector	Symmetric variables	Vector	Antisymmetric variables
$\{\mathfrak{E}\}_n$	$\varepsilon_{s,n}$, $\varepsilon_{\theta,n}$, $-2\bar{\varepsilon}_{s\theta,n}$, $\kappa_{s,n}$, $\kappa_{\theta,n}$, $-2\bar{\kappa}_{s\theta,n}$, $2\varepsilon_{s3,n}$, $-2\bar{\varepsilon}_{\theta 3,n}$	$\{E\}_n$	$\bar{\varepsilon}_{s,n}$, $\bar{\varepsilon}_{\theta,n}$, $2\varepsilon_{s\theta,n}$, $\bar{\kappa}_{s,n}$, $\bar{\kappa}_{\theta,n}$, $2\kappa_{s\theta,n}$, $2\bar{\varepsilon}_{s3,n}$, $2\varepsilon_{\theta 3,n}$
$\{\mathfrak{H}\}_n$	$N_{s,n}$, $N_{\theta,n}$, $-\bar{N}_{s\theta,n}$, $M_{s,n}$, $M_{\theta,n}$, $-\bar{M}_{s\theta,n}$, $Q_{s,n}$, $-\bar{Q}_{\theta,n}$	$\{H\}_n$	$\bar{N}_{s,n}$, $\bar{N}_{\theta,n}$, $N_{s\theta,n}$, $\bar{M}_{s,n}$, $\bar{M}_{\theta,n}$, $M_{s\theta,n}$, $\bar{Q}_{s,n}$, $Q_{\theta,n}$
$\{\mathfrak{X}\}_n$	u_n, $\bar{v}_n$, w_n, $\phi_{s,n}$, $\bar{\phi}_{\theta,n}$	$\{X\}_n$	$\bar{u}_n$, $-v_n$, $\bar{w}_n$, $\bar{\phi}_{s,n}$, $-\phi_{\theta,n}$
$\{\mathfrak{Q}\}_n$	$p_{s,n}$, $\bar{p}_{\theta,n}$, p_n, $m_{s,n}$, $\bar{m}_{\theta,n}$	$\{Q\}_n$	$\bar{p}_{s,n}$, $-p_{\theta,n}$, $\bar{p}_n$, $\bar{m}_{s,n}$, $-m_{\theta,n}$

Table 3.- Symmetric and Antisymmetric Tire Quantities

[$n = 0$]

Vector	Symmetric variables	Vector	Antisymmetric variables
$\{\mathfrak{E}\}_0$	$\varepsilon_{s,0}$, $\varepsilon_{\theta,0}$, $\kappa_{s,0}$, $\kappa_{\theta,0}$, $2\varepsilon_{s3,0}$	$\{E\}_0$	$2\varepsilon_{s\theta,0}$, $2\kappa_{s\theta,0}$, $2\varepsilon_{\theta 3,0}$
$\{\mathfrak{H}\}_0$	$N_{s,0}$, $N_{\theta,0}$, $M_{s,0}$, $M_{\theta,0}$, $Q_{s,0}$	$\{H\}_0$	$N_{s\theta,0}$, $M_{s\theta,0}$, $Q_{\theta,0}$
$\{\mathfrak{X}\}_0$	u_0, w_0, $\phi_{s,0}$	$\{X\}_0$	$-v_0$, $-\phi_{\theta,0}$
$\{\mathfrak{Q}\}_0$	$p_{s,0}$, p_0, $m_{s,0}$	$\{Q\}_0$	$-p_{\theta,0}$, $-m_{\theta,0}$

Table 4.- Amplitudes of Global Approximation Vectors in Proposed Strategy

[Two-layered anisotropic toroidal shell subjected to normal pressure loading $p = p_o \cos n\theta$ (see fig. 6)]

Number of vectors	ψ_1	ψ_2	ψ_3	ψ_4	ψ_5	ψ_6	ψ_7	ψ_8
n = 0								
4	0.9902	0.9902	1.0630	0.3543				
6	1.0005	1.0005	.3595	.1198	0.1463	2.397×10^{-2}		
8	1.00	1.00	.6221	.2074	-5.963×10^{-2}	-1.308×10^{-2}	8.517×10^{-3}	1.217×10^{-3}
n = 2								
4	0.9954	0.9954	1.0327	0.3442				
6	1.0015	1.0015	.1544	.0515	0.1198	2.927×10^{-2}		
8	.9996	.9996	.6473	.2158	-6.541×10^{-2}	-1.193×10^{-2}	7.974×10^{-3}	1.139×10^{-3}
Taylor series	1.00	1.00	0.50	0.1667	4.167×10^{-2}	8.333×10^{-3}	1.389×10^{-3}	1.984×10^{-4}

Table 5.- Accuracy and Convergence of Solutions Obtained With Proposed Strategy for Orthotropic Tire Subjected to Uniform Inflation Pressure and Unsymmetric Localized Loading

[See fig. 12; for uniform inflation pressure only $(q_1 = q_2 = 0)$,

$$\frac{w_c}{h} = \frac{w_b}{h} = 0.08935 \quad \text{and} \quad \frac{U}{E_L h^3} = 0.3633$$

]

Number of approximation vectors	$\frac{w_c}{h}^*$	$10 \times \frac{w_b}{h}^*$	$\frac{U}{E_L h^3}$
3	-0.6430	0.8820	0.3464
6	-.6499	.8907	.3572
10	-.6548	.8896	.3570
15	-.6569	.8842	.3568
21	-.6554	.8917	.3569
Direct finite-element solution	-0.6553	0.8918	0.3569

*See figure 3.

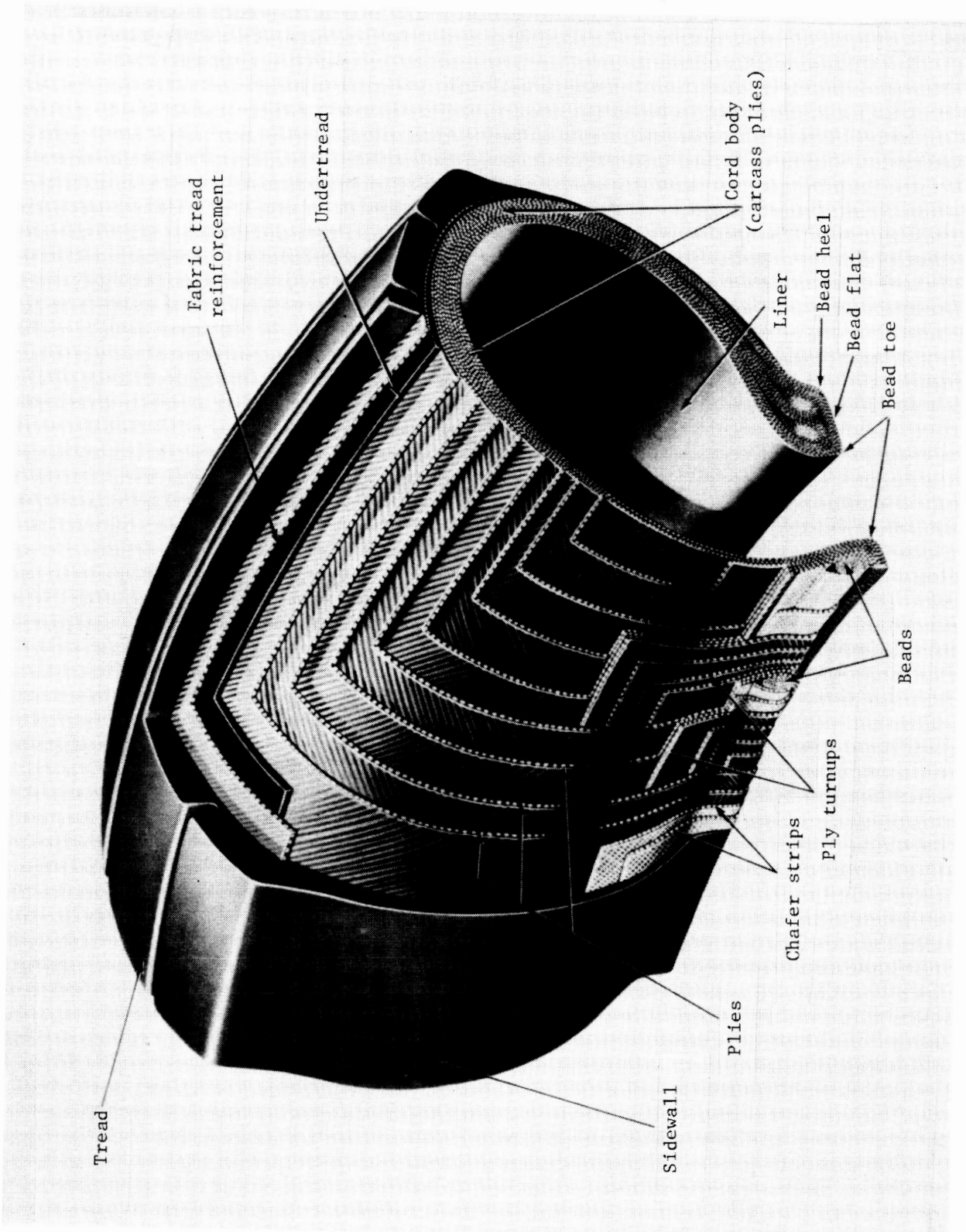

Figure 1.- Components of an aircraft tire.

Figure 2.- Tire model and sign convention of stress resultants, generalized displacements, and external loading.

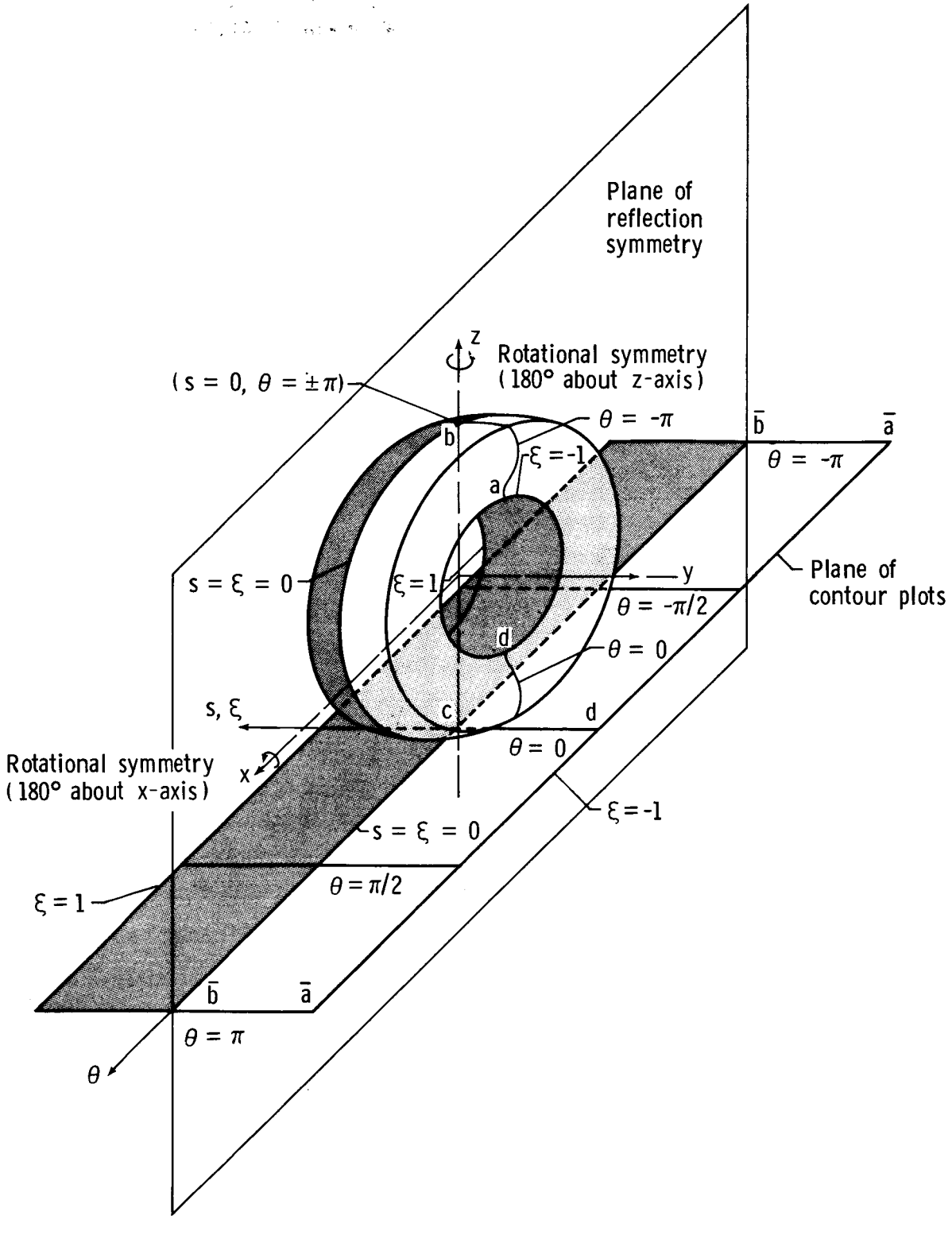

Figure 3.- Axes of rotational symmetry and plane-of-reflection symmetry for tires.

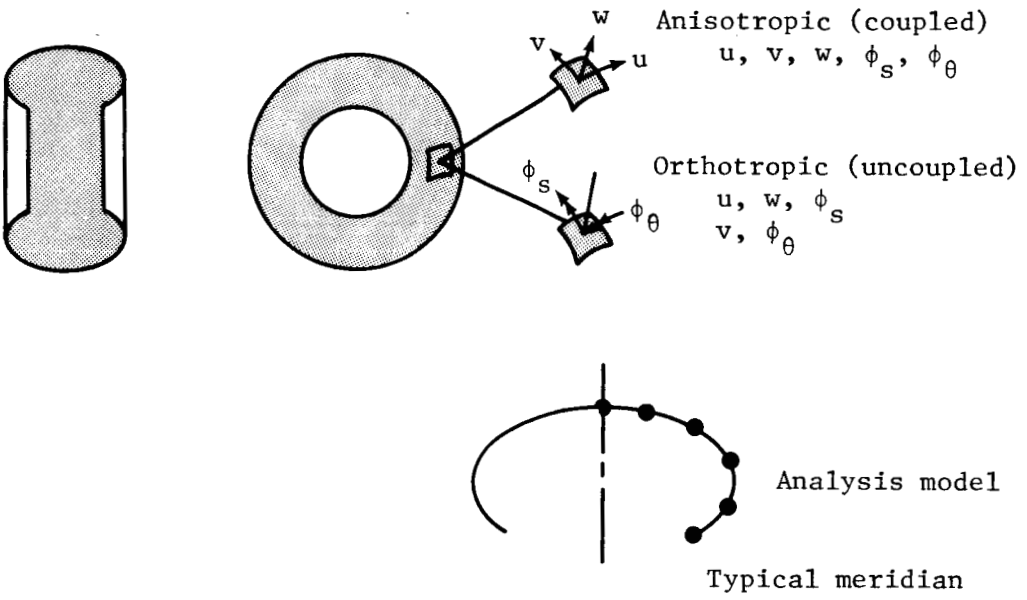

Figure 4.- Axial symmetry for orthotropic and anisotropic tires.

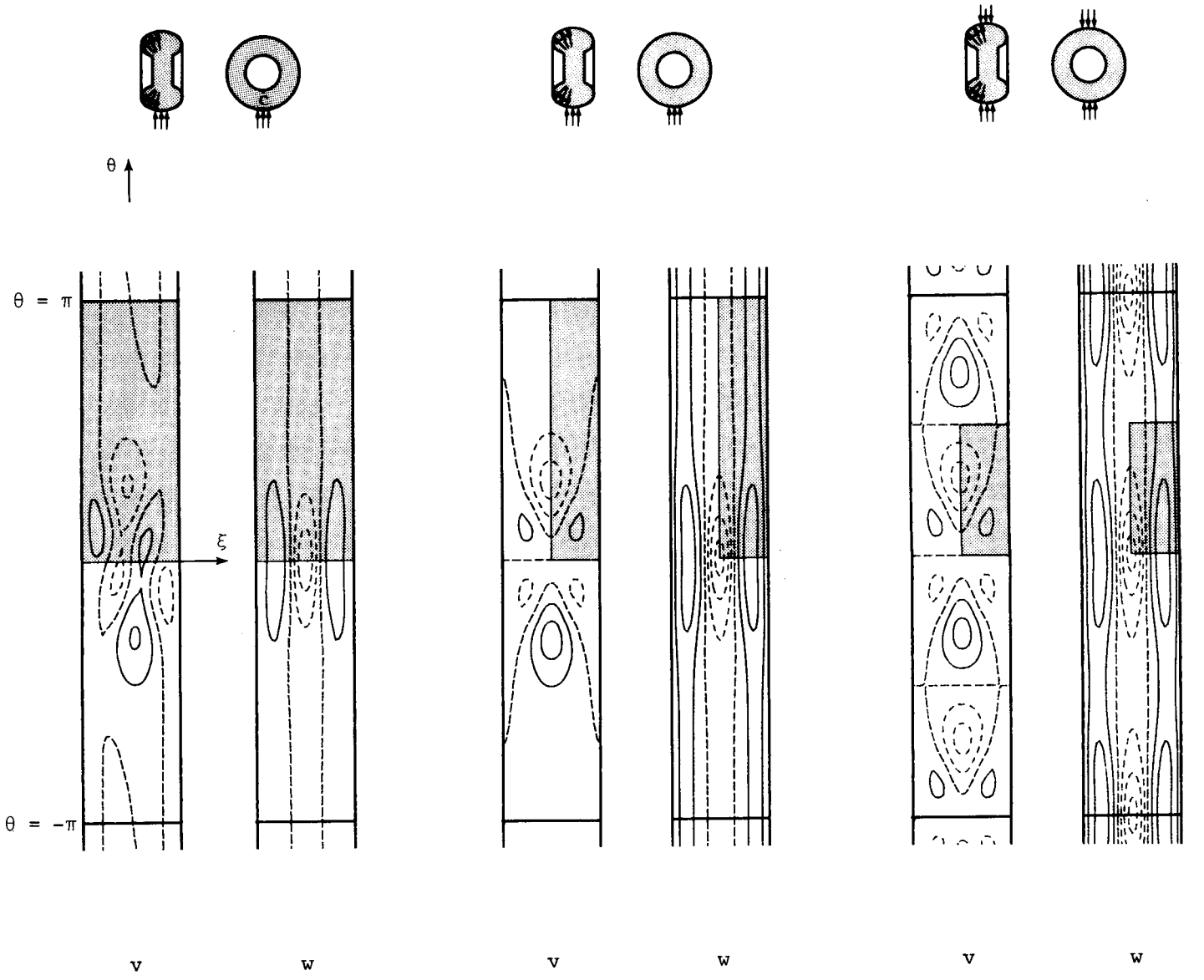

(a) Anisotropic tire with rotational symmetry.

(b) Orthotropic tire with reflection symmetry.

(c) Orthotropic tire with periodic symmetry.

Figure 5.- Rotational, reflection, and periodic symmetries for tires subjected to inflation pressure and localized normal loading. Analysis regions shown shaded.

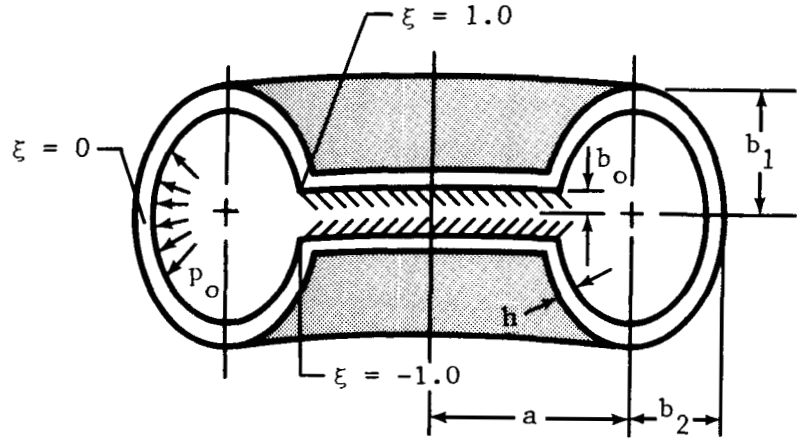

E_L = 517 MPa (7.5×10^4 psi)
E_T = 8.27 MPa (1.2×10^3 psi)
G_{LT} = 3.10 MPa (450 psi)
G_{TT} = 1.86 MPa (270 psi)
ν_{LT} = 0.4
h = 1.067 cm (0.42 in.)
b_o = 5.08 cm (2.0 in.)
b_1 = 6.223 cm (2.45 in.)
b_2 = 5.385 cm (2.12 in.)
a = 19.558 cm (7.70 in.)

Number of layers = 2
Fiber orientation: $[+55^\circ/-55^\circ]$

Figure 6.- Laminated, anisotropic elliptical toroidal shell used in the present study.

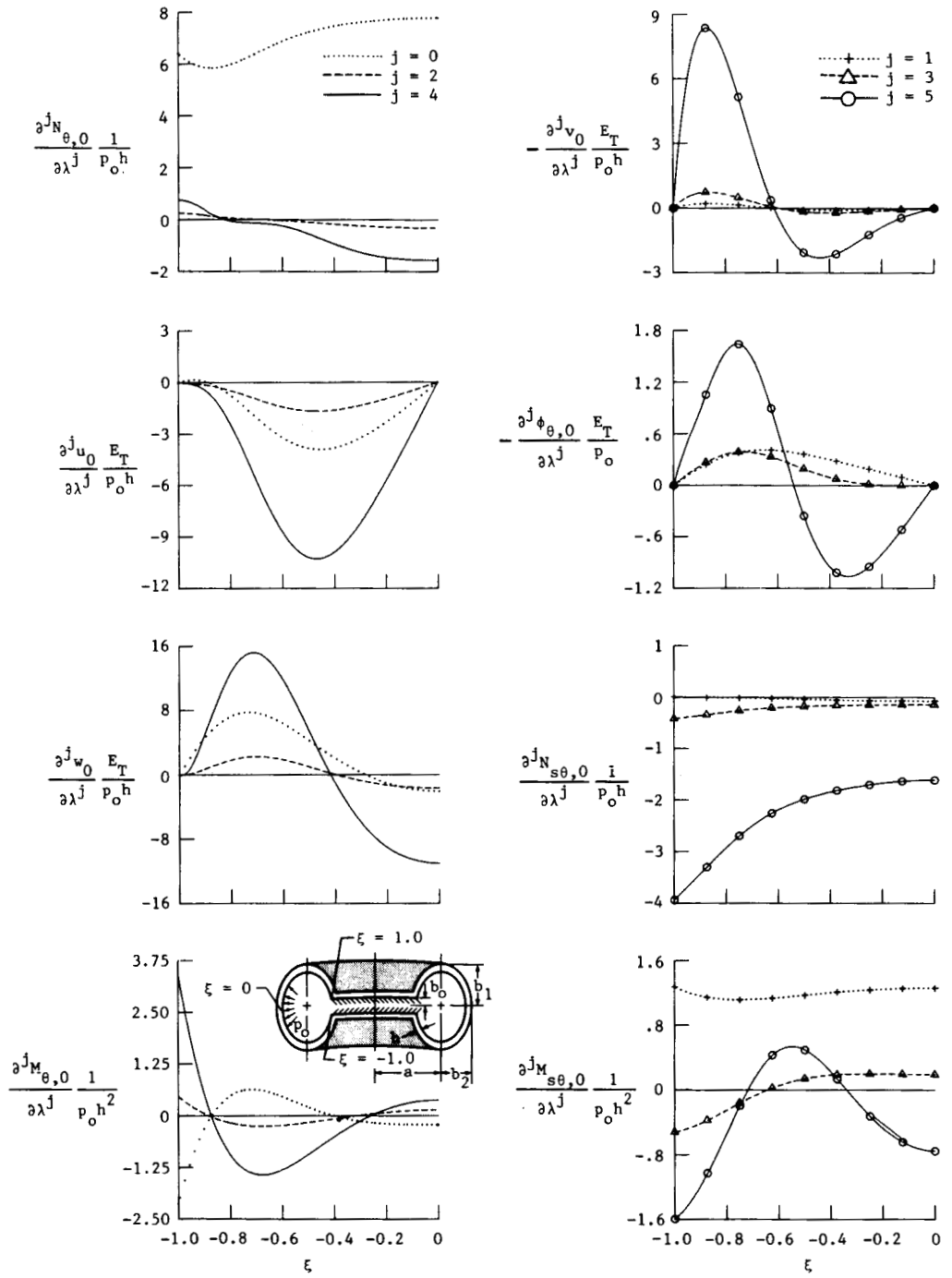

(a) Even-order derivatives.

(b) Odd-order derivatives.

Figure 7.- Global approximation vectors used with semianalytic finite elements for two-layered anisotropic tire subjected to normal loading. n = 0.

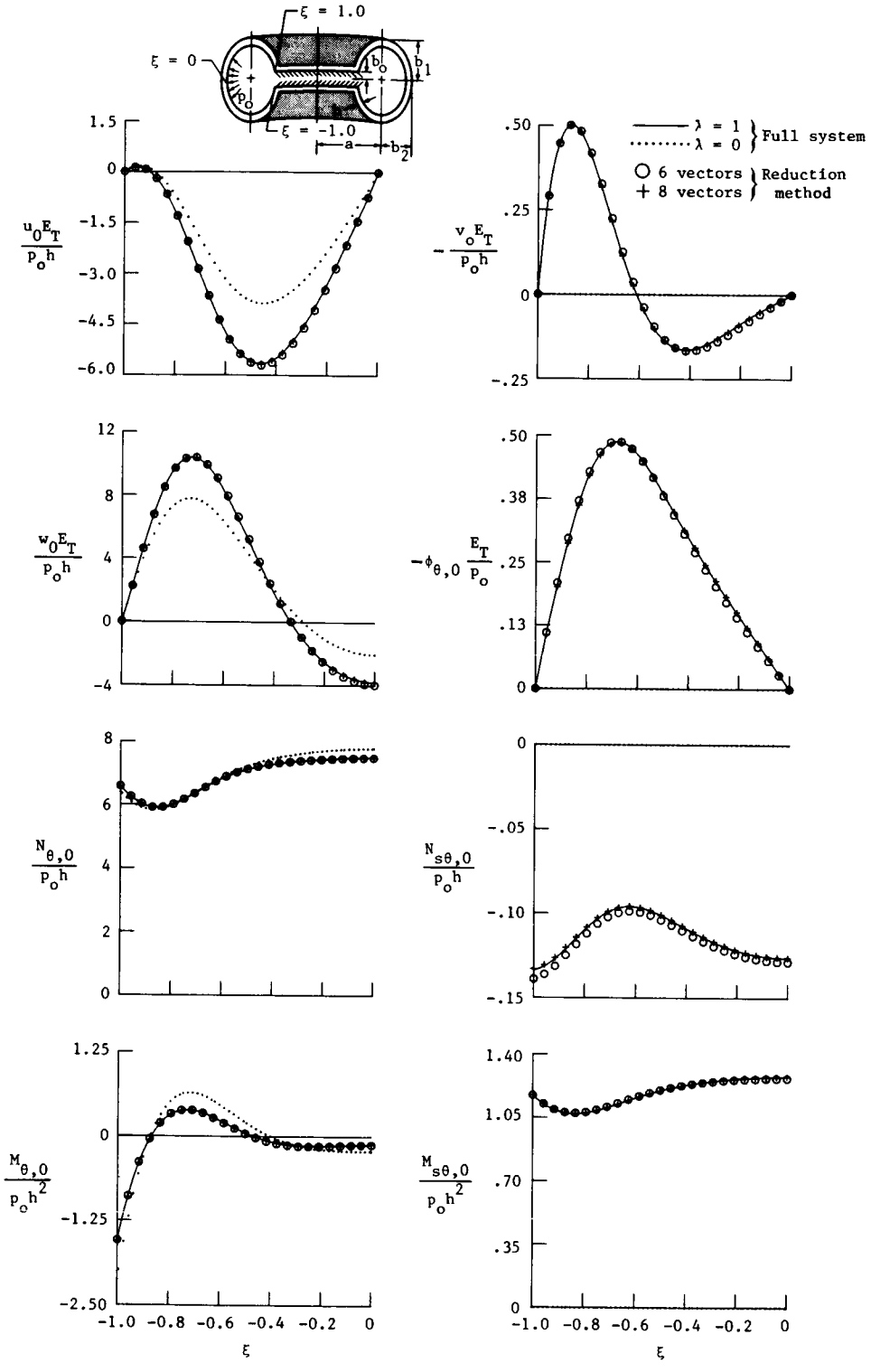

(a) Symmetric quantities. (b) Antisymmetric quantities.

Figure 8.- Accuracy of solutions obtained with proposed strategy for two-layered anisotropic tire subjected to normal loading and modeled by semianalytic finite elements and n = 0.

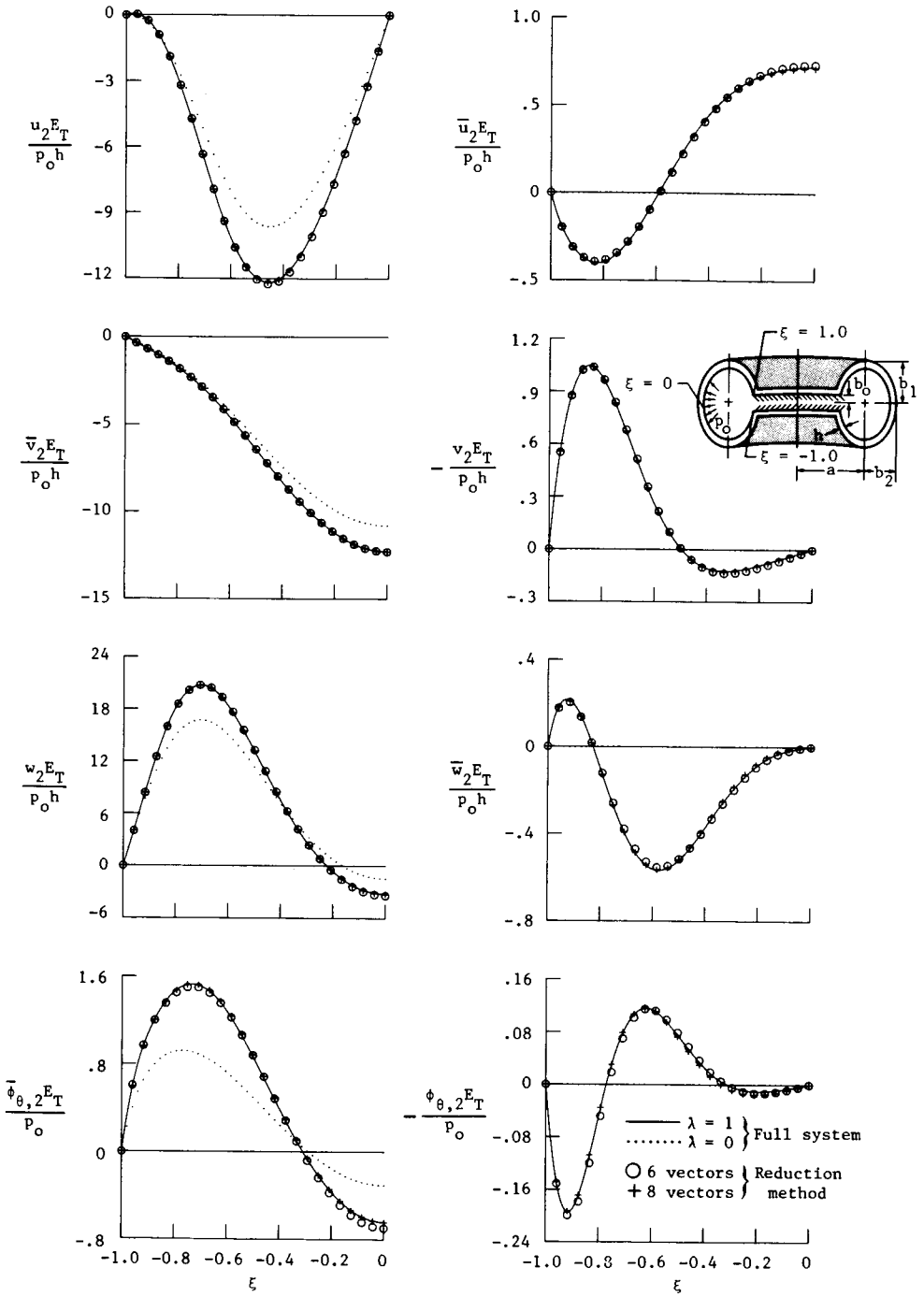

(a) Symmetric generalized displacements.

(b) Antisymmetric generalized displacements.

Figure 9.- Accuracy of solutions obtained with proposed strategy for two-layered anisotropic tire subjected to normal loading and modeled by semianalytic finite elements and $n = 2$. $p = p_o \cos 2\theta$.

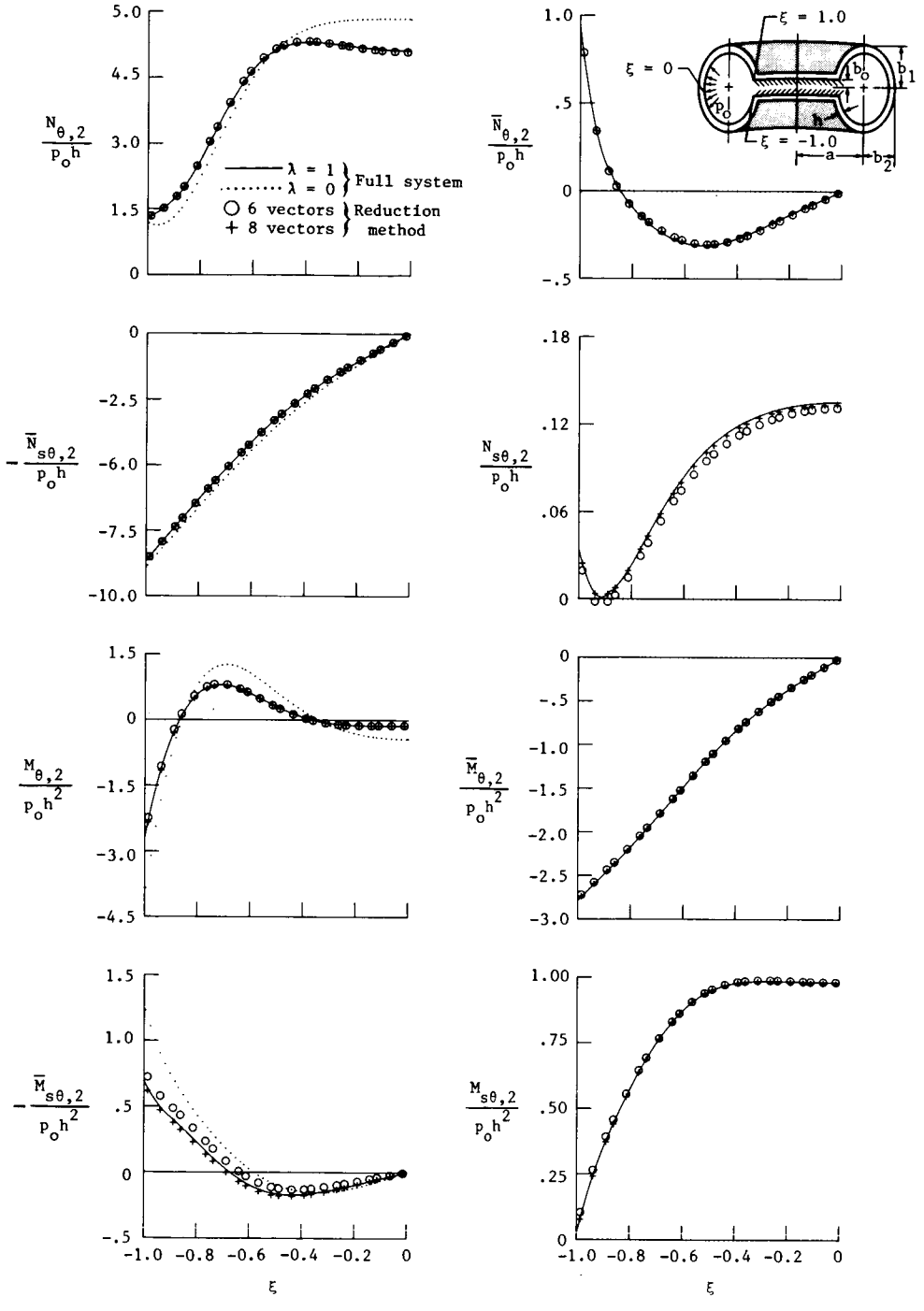

(c) Symmetric stress resultants.

(d) Antisymmetric stress resultants.

Figure 9.- Concluded.

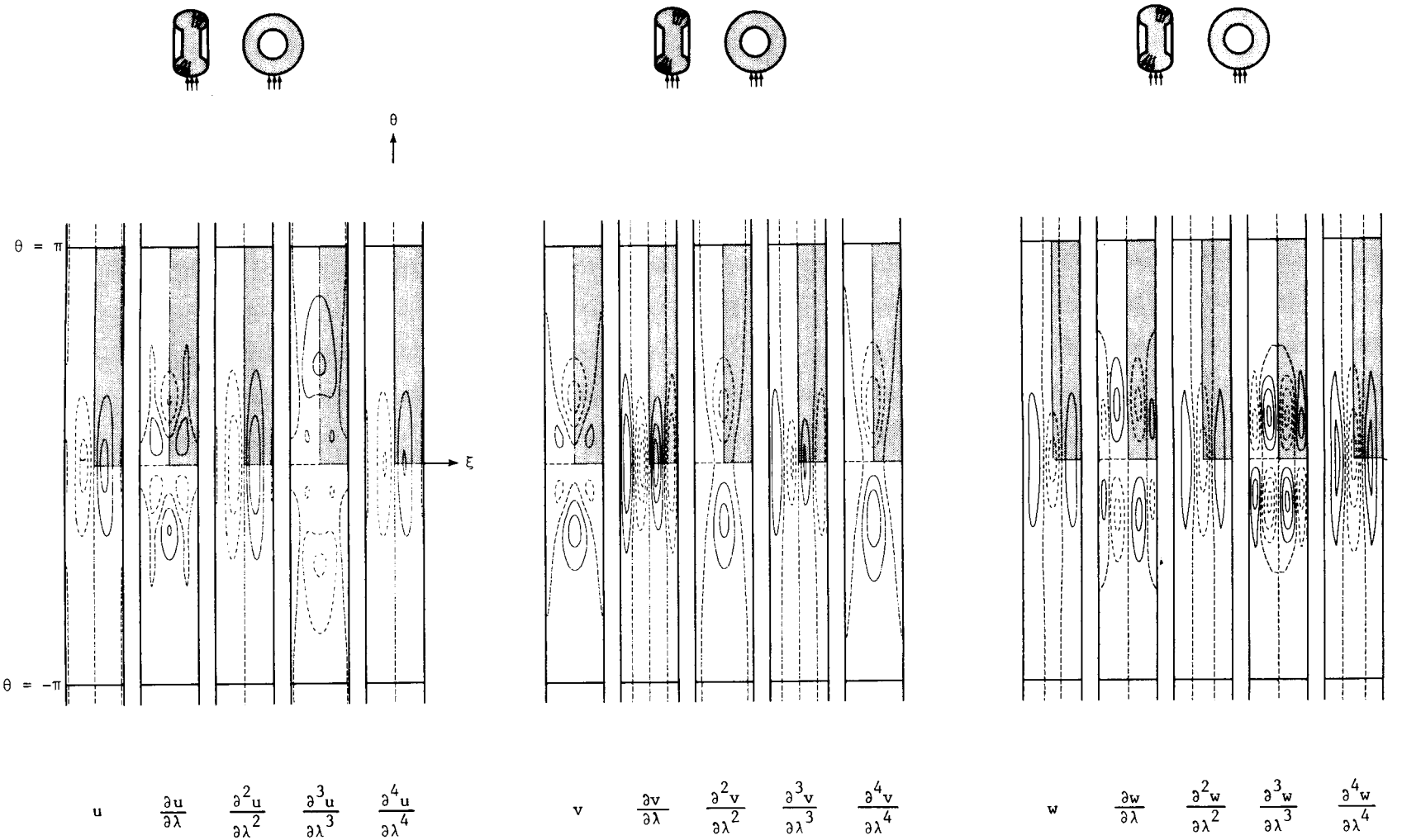

Figure 10.- Normalized contour plots for global approximation vectors for two-layered anisotropic tire subjected to uniform inflation pressure and localized loading. Each plot is divided by maximum absolute value of the function.

Figure 10.- Concluded.

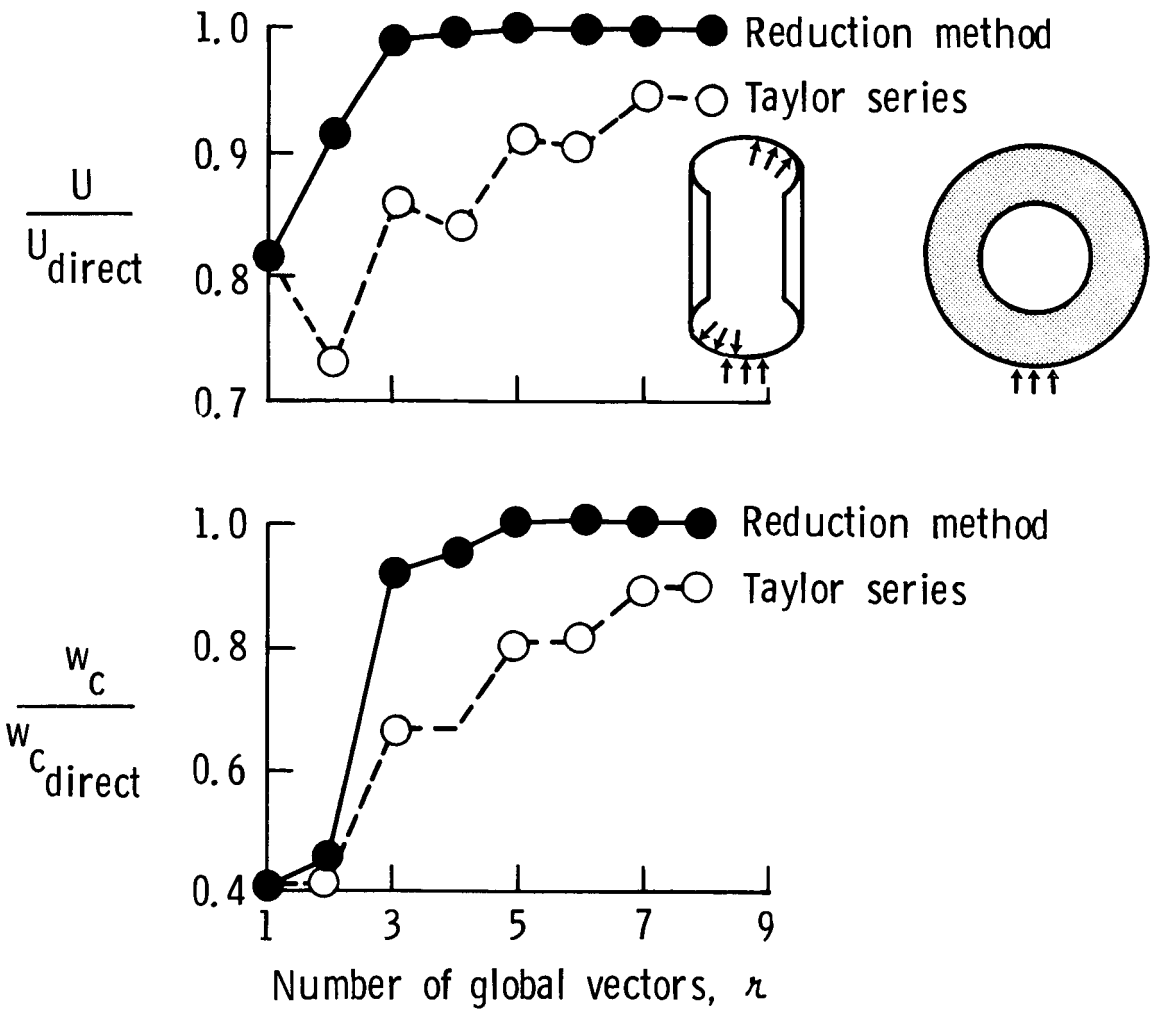

Figure 11.- Convergence of maximum normal displacement w_c and total strain energy U obtained with proposed strategy and with Taylor series expansion for two-layered anisotropic tire subjected to localized loading.

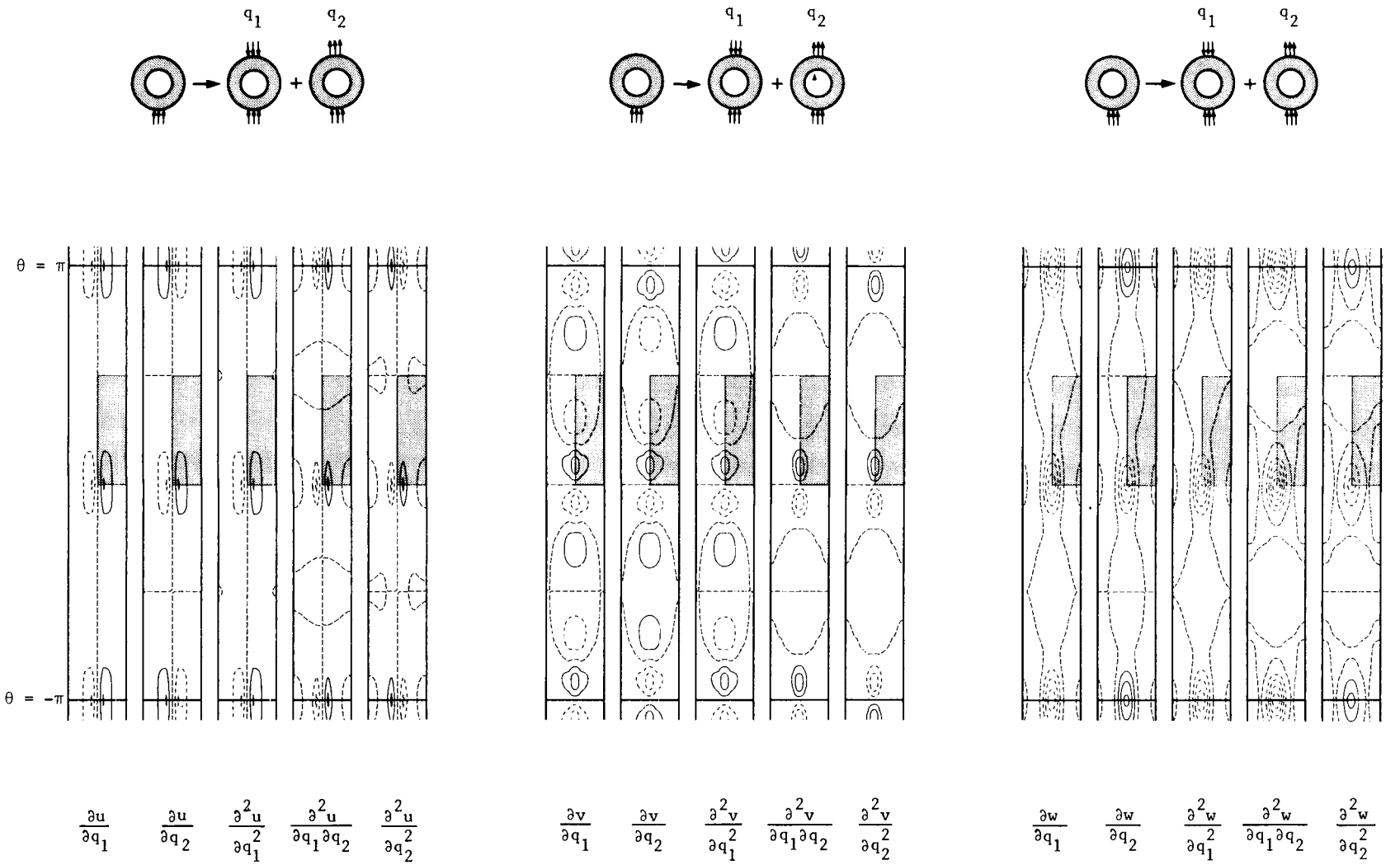

Figure 12.- Normalized contour plots for global approximation vectors for two-layered orthotropic tire subjected to combined uniform inflation pressure and symmetric or antisymmetric localized loadings.

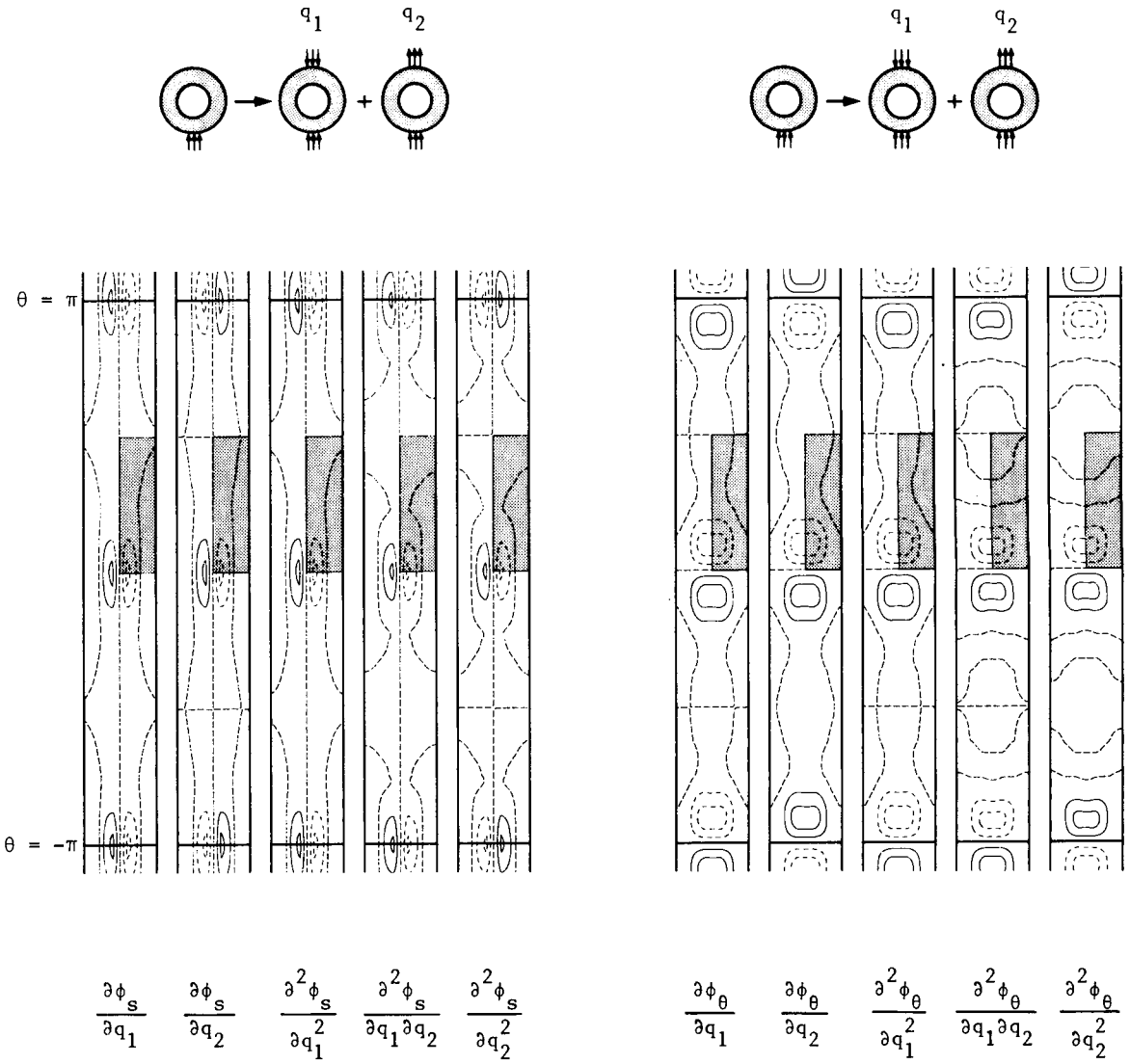

Figure 12.- Concluded.

Standard Bibliographic Page

1. Report No.	2. Government Accession No.	3. Recipient's Catalog No.
NASA TP-2649		

4. Title and Subtitle	5. Report Date
Exploiting Symmetries in the Modeling and Analysis of Tires	March 1987
	6. Performing Organization Code 505-63-41-02
7. Author(s)	8. Performing Organization Report No.
Ahmed K. Noor, Carl M. Andersen, and John A. Tanner	L-16185
9. Performing Organization Name and Address	10. Work Unit No.
Langley Research Center Hampton, VA 23665-5225	11. Contract or Grant No.
12. Sponsoring Agency Name and Address	13. Type of Report and Period Covered
National Aeronautics and Space Administration Washington, DC 20546-0001	Technical Paper
	14. Sponsoring Agency Code

15. Supplementary Notes

Ahmed K. Noor: The George Washington University, Joint Institute for Advancement of Flight Sciences, Langley Research Center, Hampton, Virginia.
Carl M. Andersen: The College of William and Mary, Williamsburg, Virginia; work performed under cooperative agreement NCCI-40.
John A. Tanner: Langley Research Center, Hampton, Virginia.

16. Abstract

This paper presents a simple and efficient computational strategy for reducing both the size of a tire model and the cost of the analysis of tires in the presence of symmetry-breaking conditions (unsymmetry in the tire material, geometry, or loading). The strategy is based on approximating the unsymmetric response of the tire with a linear combination of symmetric and antisymmetric global approximation vectors (or modes). Details are presented for the three main elements of the computational strategy, which include: use of special three-field mixed finite-element models, use of operator splitting, and substantial reduction in the number of degrees of freedom. The proposed computational strategy is applied to three quasi-symmetric problems of tires: linear analysis of anisotropic tires through use of semianalytic finite elements, nonlinear analysis of anisotropic tires through use of two-dimensional shell finite elements, and nonlinear analysis of orthotropic tires subjected to unsymmetric loading. Three basic types of symmetry (and their combinations) exhibited by the tire response are identified.

17. Key Words (Suggested by Authors(s))	18. Distribution Statement
Tire response Nonlinear analysis of tires Linear analysis of tires Sanders-Budiansky shell theory Semianalytical finite elements Tire symmetries Orthotropic tires Anisotropic tires	Unclassified - Unlimited Subject Category 05

19. Security Classif.(of this report)	20. Security Classif.(of this page)	21. No. of Pages	22. Price
Unclassified	Unclassified	61	A04

For sale by the National Technical Information Service, Springfield, Virginia 22161

NASA-Langley, 1987